Lawrence Berkeley National Laboratory
Recent Work

Title
SUBLIMATION KINETICS OF ZINC SINGLE CRYSTALS

Permalink
https://escholarship.org/uc/item/93w2p8j0

Author
Mar, Raymond Wing.

Publication Date
1968-05-01

eScholarship.org Powered by the California Digital Library
University of California

UCRL-18257

University of California

Ernest O. Lawrence Radiation Laboratory

TWO-WEEK LOAN COPY

This is a Library Circulating Copy which may be borrowed for two weeks. For a personal retention copy, call Tech. Info. Division, Ext. 5545

SUBLIMATION KINETICS OF ZINC SINGLE CRYSTALS

Raymond Wing Mar

(Ph. D. Thesis)

May 1968

RECEIVED
RADIATION LABORATORY
JUL 25 1968
LIBRARY AND DOCUMENTS SECTION

Berkeley, California

UCRL-18257

DISCLAIMER

This document was prepared as an account of work sponsored by the United States Government. While this document is believed to contain correct information, neither the United States Government nor any agency thereof, nor the Regents of the University of California, nor any of their employees, makes any warranty, express or implied, or assumes any legal responsibility for the accuracy, completeness, or usefulness of any information, apparatus, product, or process disclosed, or represents that its use would not infringe privately owned rights. Reference herein to any specific commercial product, process, or service by its trade name, trademark, manufacturer, or otherwise, does not necessarily constitute or imply its endorsement, recommendation, or favoring by the United States Government or any agency thereof, or the Regents of the University of California. The views and opinions of authors expressed herein do not necessarily state or reflect those of the United States Government or any agency thereof or the Regents of the University of California.

UCRL-18257

UNIVERSITY OF CALIFORNIA

Lawrence Radiation Laboratory
Berkeley, California

AEC Contract No. W-7405-eng-48

SUBLIMATION KINETICS OF ZINC SINGLE CRYSTALS

Raymond Wing Mar

(Ph. D. Thesis)

May, 1968

Contents

SUBLIMATION KINETICS OF ZINC SINGLE CRYSTALS

Raymond Wing Mar

Inorganic Materials Research Division, Lawrence Radiation Laboratory, and Department of Mineral Technology, College of Engineering, University of California, Berkeley, California

May, 1968

ABSTRACT

The kinetics of the free surface sublimation of zinc single crystals were investigated using the torsion-Langmuir technique in conjunction with optical and electron microscopes. Sublimation from cleaved surfaces took place in two distinct stages, a stage of pressure increase with time followed by a stage in which steady state pressures were measured. The first stage was correlated with the formation of thermal pits on the surface and the subsequent increase in dimensions of the pits. Thermal pits formed at places where dislocations intersected the surface, but only one out of every 10 to 20 dislocations, as measured by chemical etching formed thermal pits. The cleaved surface was found to hinder the motion of the evaporation ledges. This hinderance is probably a result of strong adsorption of contaminants on the cleaved surface.

Steady state pressures were attained once the original cleaved surface had been eliminated by the spreading and coalescing thermal pits. Rates of steady state sublimation were determined over the temperature range 525°K to 660°K. The evaporation coefficient, α, was found to be unity for the (0001) surface of high purity zinc and the $(10\bar{1}0)$ surface of less pure zinc. The (0001) surface was characterized by dislocation densities ranging from 3×10^4 to 2×10^5 lines/cm^2. These results

contradict the prediction made by Hirth and Pound that α equals 1/3 for low index surfaces which have dislocation densities less than 10^6 lines/cm^2.

Zinc oxide formed in discrete patches on the surface by the reaction

$$Zn(s) + 1/2\ O_2(g) \rightarrow ZnO(s).$$

The sublimation flux and surface morphology were surprisingly insensitive to the presence of the oxide particles. On the other hand, the effect of bulk impurities on the rate of sublimation and the surface morphology was apparently quite significant. While the zinc with no detectable impurities yielded $\alpha = 1$, less pure (99.9987%) zinc had an evaporation coefficient for the (0001) plane of 0.74 ± 0.1. The (0001) surfaces of high purity zinc resembled flat plains with networks of interconnecting ridges in areas where zinc oxide collected. The (0001) surfaces of the less pure zinc were pitted and ledged. The nature of the surface features on the (0001) and (1010) planes for the two types of zinc which develop during sublimation are described in detail.

I. INTRODUCTION

The sublimation of solids has been investigated theoretically and experimentally for many years, and there is still no generally accepted theory of evaporation kinetics. The degree of mechanistic complexity varies greatly depending upon the nature of the reaction. One would expect marked differences between the sublimation mechanisms of monatomically subliming metals, compounds which dissociate or associate upon sublimation, and systems which sublime incongruently. Even the mechanism for the simplest of these processes, the monatomic sublimation of metals, is not firmly established.

A traditional approach to the problem of sublimation is to search for an expression for α, the evaporation coefficient, where α is defined as the ratio of the evaporating flux from a surface to the gross flux under equilibrium conditions. At this time, it will be of benefit to explore the inception of the coefficient.

Hertz[1] was the first to formulate a theoretical expression for the rate of evaporation when he noted that the upper limit to the rate is

$$J = \frac{\bar{\nu} n_e}{4} = \frac{P_e}{(2\pi mkT)^{1/2}} \qquad (a)$$

This expression was derived on the assumption that the maximum rate of evaporation can never be larger than the rate at which molecules strike the condensate under equilibrium conditions.

In 1915, Knudsen[2] found that the experimental rate of evaporation of mercury was at least three orders of magnitude less than that predicted from the Hertz equation. He therefore introduced the quantity α, the

evaporation coefficient, into equation (a) so that the actual rate of evaporation would be expressed as

$$J = \frac{\alpha \bar{\nu} n_e}{4} = \frac{\alpha P_e}{(2\pi mkT)^{1/3}} \qquad (b)$$

which is the well known Hertz-Knudsen equation. It is seen that the original historical definition of α, is the ratio of the observed rate of evaporation in vacuo to the maximum rate as calculated from the Hertz equation.

Evaporation coefficients are useful as correction factors for calculations of the flux of molecules escaping from a surface. In many cases the free surface flux is much less than that expected from equilibrium pressure data.[3-5] However, the coefficient provides no insight into the mechanistic details of the evaporation process.

Many theoretical attempts have been made to define the evaporation coefficient. The development of the theory for the sublimation of metals is based primarily on the concepts as set forth by Volmer.[6] Volmer postulated that molecules sublime via a stepwise process by movement from the bulk to surface sites of successively lower binding energy. These various surface sites have been envisioned by Kossel[7] and Stranski,[8] and their concept of the close packed surface is illustrated in Fig. 1.

Volmer's stepwise concept of sublimation has been examined mathematically by Knacke and Stranski[10] and more extensively by Hirth and Pound.[10-12] The basic assumption made by Hirth and Pound is that the rate determining steps in the sublimation process are the reactions:

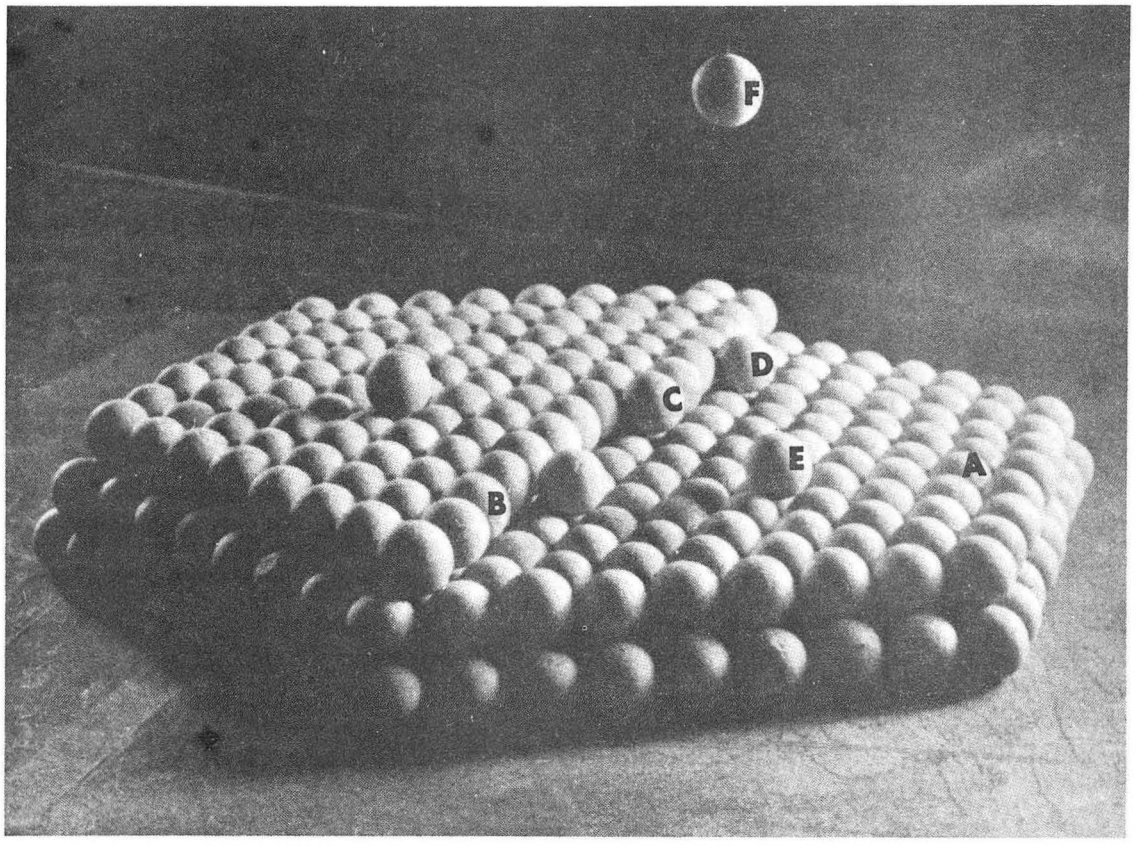

XBB 687-4159

A - atom in surface
B - atom in ledge
C - atom in kink
D - atom at ledge
E - adsorbed atom
F - vapor atom

Fig. 1 Kossel-Stranski model of a close-packed surface (ref. 9).

atoms at ledge → adsorbed atoms (c)

adsorbed atoms → vapor (d)

All reactions prior to the first reaction, i.e. the atoms in ledge → atoms in kink and atoms in kink → atoms at ledge, are assumed to be very rapid so that equilibrium concentrations are maintained for these atom sites. All other paths of escape into the vapor phase, i.e. atoms in ledge → vapor, atoms in kink → vapor, etc. are assumed to be negligible. Finally, it is assumed that the concentration of adsorbed atoms at the ledges is always maintained at the equilibrium concentration.

The prediction of the analysis then is that the evaporation process is maintained by surface diffusion from ledges followed by evaporation from surface adsorption sites.

Hirth and Pound[11] have shown that for a perfect crystal,

$$\alpha = \frac{2}{Q\lambda} \tanh \frac{Q\lambda}{2} + \left(1 - \frac{2}{Q\lambda}\right) \frac{P}{P_e} \qquad (e)$$

where Q is a constant given by $(C/D_s)^{1/2}$ where D_s is the surface diffusivity, and C is equal to $\nu e^{-\Delta F_1/kT}$. ν is the vibrational frequency of an atom on the surface, and ΔF_1 is the free energy of activation for the desorption process. λ is the distance between adjacent parallel ledges.

A study of the dynamics of ledge behavior on a perfect crystal shows that the edges of the crystal are a very ready source of ledges.[11] The ledge to ledge spacing between adjacent parallel ledges reaches a limiting value of approximately $\lambda = 6/Q$. This limiting value is somewhat arbitrarily chosen as the distance at which the rate change in

ledge velocity is one one-hundredth of the maximum ledge velocity. This limiting condition imposes a limiting value on α of

$$\alpha = \frac{1}{3} + \frac{P}{P_e}\frac{2}{3} \qquad (f)$$

P is the background pressure, and P/P_e is usually zero under ordinary vacuum evaporation conditions.

A very important question is to what extent crystal imperfections inherently present in real crystals will affect α. Hirth and Pound have discussed such effects as pores, grain boundaries, and cracks.[11,12] The defects of greatest predicted effect on evaporation kinetics are dislocations intersecting the surface with a major screw orientation because screw dislocations act as efficient sources for ledges. Hirth and Pound estimated that at concentrations in excess of 10^6 cm^{-2}, screw dislocations can increase α in vacuo from 1/3, as otherwise predicted, to unity.[13]

The role of screw dislocations in the process of condensation has been extensively studied. It has been shown that the generation of spiral growth rings at screw dislocations can produce crystal growth from the vapor phase at vapor saturations which according to nucleation and growth theory should be otherwise ineffective.[14-16]

Evaporation about a screw dislocation has been mathematically analyzed by Cabrera and Levine.[17] The evaporation steps are expected to be essentially the reverse of those followed in growth at spiral dislocations.

Reported values of α for metals generally line in the range between

0.1 and 1.0.[18,19] Various investigations have reported coefficients of less than unity for silver,[20,21] beryllium,[22,23] gold,[24] tellurium,[25] and titanium,[26] however, in all cases there are reasons to question the validity of the reported values. For silver[27,28] and beryllium,[29] values of unity have been reported by other investigators. Edwards, Johnston, and Ditmars[30] find α to be unity for titanium, and feel that Carpenter and Mair's data are in error because they used an incorrect emissivity value. Although Metzger[25] quotes a value of $\alpha = .4$ for tellurium, he admits to a large uncertainty in this value and concludes that α may lie anywhere from .1 to 1.0.

Free surface sublimation rates at unequivocally known surface temperatures are difficult to fix precisely so that impartial observers have been unconvinced that investigators who claim less uncertainty than the factor of .25 - 2.5 conceded by Metzger are being realistic.

As of 1957, Hirth and Pound considered that no existing data provided a convincing test of their prediction that α would be 1/3 for large low index crystal surfaces with low defect densities. Accordingly, they attempted their own test with silver and found $\alpha \approx 0.4$.[20] But Hirth and Winterbottom[28] subsequently found $\alpha = 1$ for silver and concluded that Hirth and Pound's results were in error because of surface contamination from poor background pressures. Hirth and Winterbottom concluded that their own data gave a value of unity because the dislocation density in their samples was high.

The present study was undertaken as an independent effort to provide experimental tests of the Hirth and Pound theory. Other than the silver

studies of Hirth, Pound and Winterbottom, no other study of monatomically subliming metallic crystal has been extensively reported. Zinc was chosen as the metal for study for a number of reasons. For zinc the only important vapor species is the atom.[31,32] The vapor pressure at temperatures below the melting point is high enough for convenient measurement. High purity zinc crystals are easy to grow. Flat surfaces relatively free of macroscopic faults can be obtained because of the easy basal cleavage of zinc at liquid nitrogen temperatures. The etch pit method can be used to determine dislocation positions and densities on the various planes.[33,34] Previous etch pit work on the basal plane of zinc had shown that dislocation densities as low as $10^4 - 10^5$ lines/cm^2 are not impossible to obtain.[34,35] Such levels, according to the Hirth and Pound theory, should be too low to raise α above the value 1/3 predicted for large, perfect, low-index surfaces.

A primary concern of this investigation was to compare the free surface sublimation rate with equilibrium pressure data collected under as closely identical conditions as possible. Systematic discrepancies between vapor pressures collected in different apparatuses are common.[36,37] Determination of free surface sublimation rates by the torsion-Langmuir technique and equilibrium effusion rates by the torsion-effusion technique[38,39] in the same vacuum system assures cancellation of most systematic errors that influence measured values of α.

II. EXPERIMENTAL

A. Apparatus

The torsion-effusion apparatus is schematically represented in Fig. 2. The furnace consisted of thirteen 80 mil tungsten hairpin heating elements arranged in a circular array 11.5 cm in diameter. Tantalum heat shields were placed above, below and surrounding the hairpins. The electrodes were water cooled copper plates and the furnace was placed in a water cooled stainless steel vacuum shell.

The torsion cells were made of high purity graphite. The cell design permitted equilibrium data and free surface sublimation data to be collected with essentially the same cell. The basic parts of the cell as illustrated in Fig. 3 are the cell block, Knudsen cells, Langmuir orifices and Knudsen orifices. Figure 4 shows the cell assemblies used to determine the equilibrium pressures and the free surface sublimation pressures. The hole in the top of the cell reduced the possibility that zinc which evaporated from the rear face of the crystal wafer might escape in a manner that would contribute significantly to the measured torque. The possibility is small for substances with α near unity; for such substances, molecules that evaporate in areas not exposed by the orifice are reflected from the graphite holding disc back onto the surface and recondense. The feature is more important in measuring the free surface flux of a substance with a very small evaporation coefficient because molecules of such a substance do not readily recondense.

B. Technique

The apparatus was used as a null point devise. When the torsion cell twisted as a result of effusion of vapor from the eccentrically

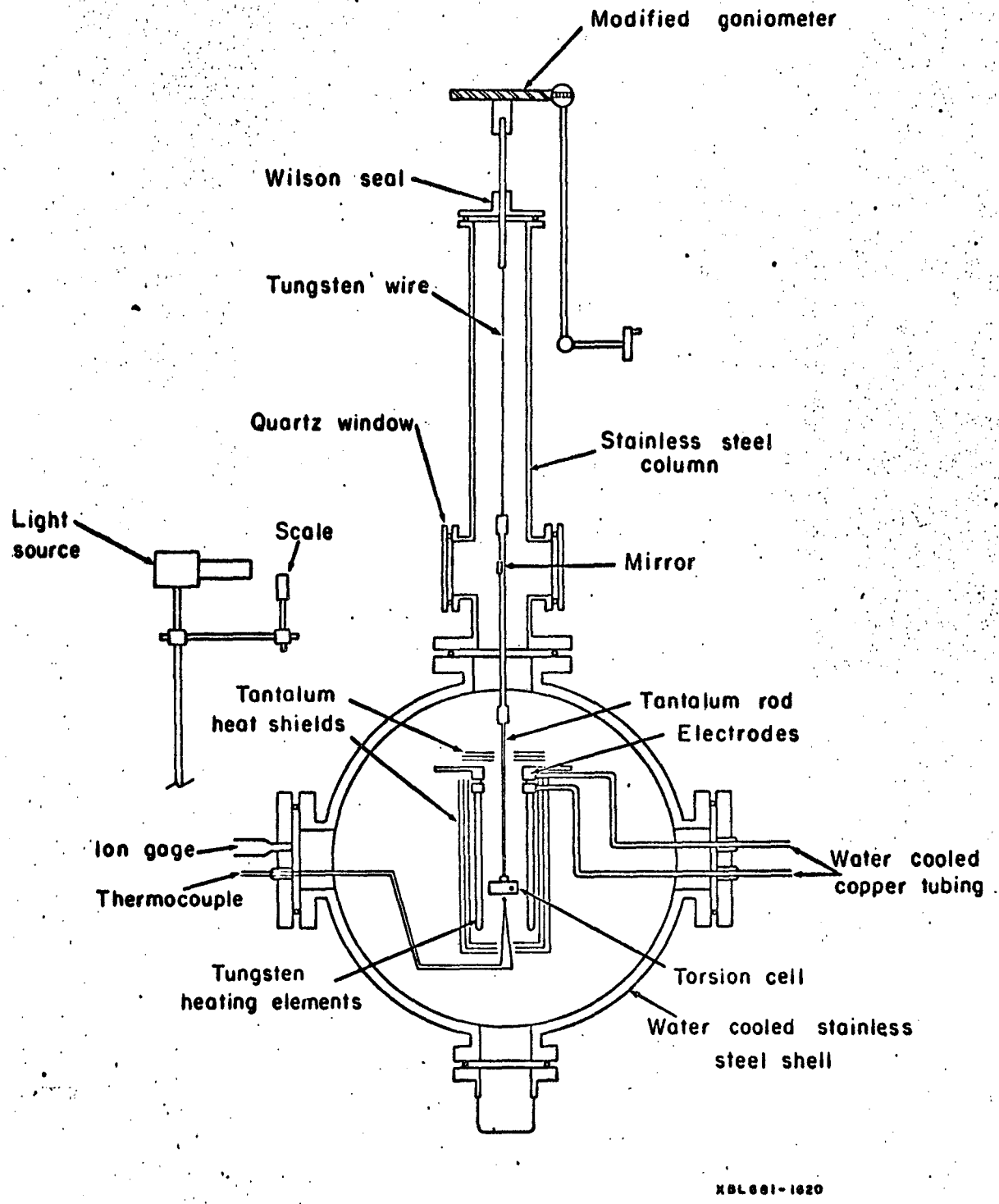

Fig. 2. Torsion effusion apparatus

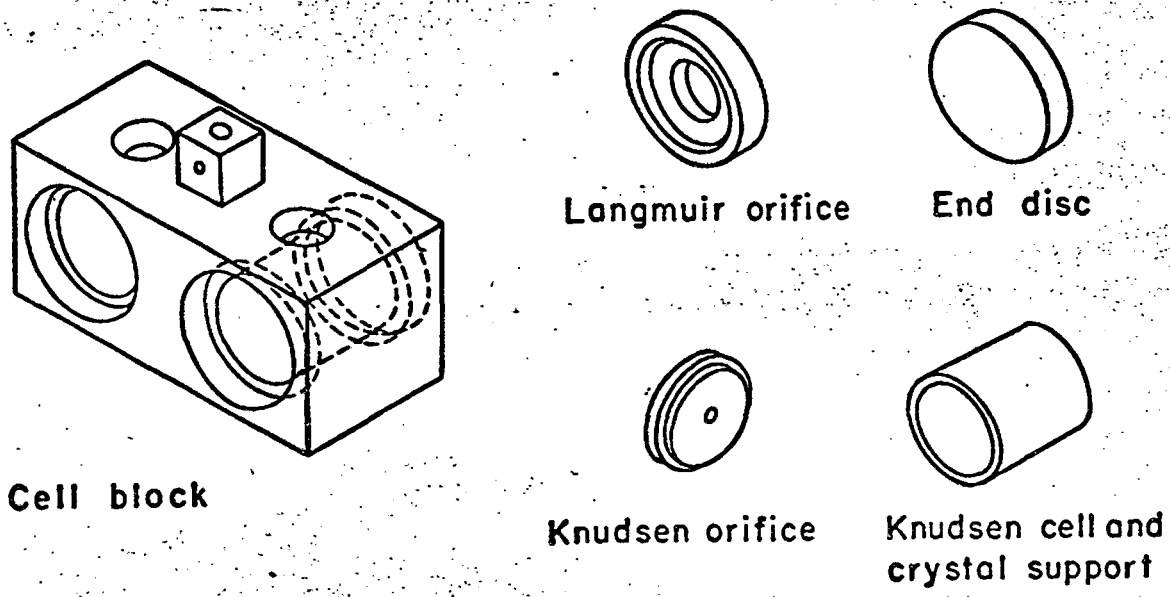

Fig. 3. Torsion cell parts

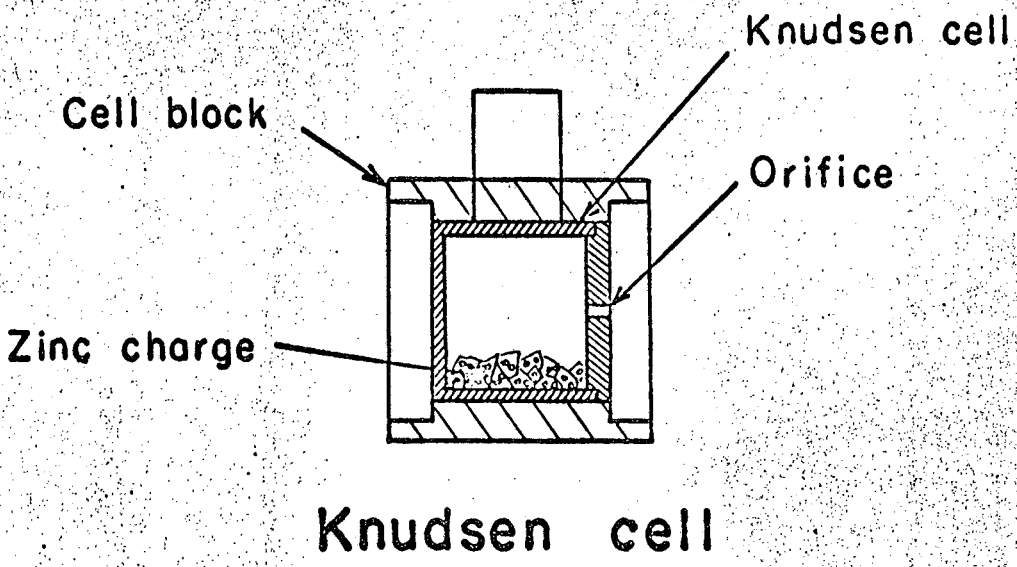

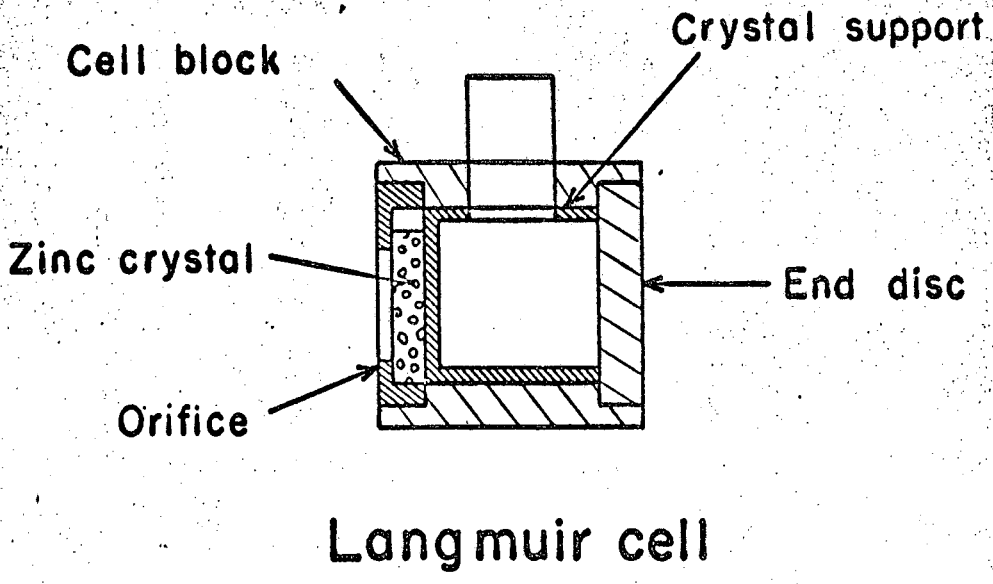

XBL684-2435

Fig. 4. Torsion cell assemblies

placed orifices, the top of the suspension system was twisted in the opposite direction to keep the cell in its original orientation. A galvanometer mirror which was attached near the top of the aluminum rod, was used in conjunction with a pinhole light beam source and a scale upon which the light beam reflected from the mirror to fix the null position. The angle of twist required to restore the cell to its null position was recorded to the nearest .001 degree by means of a modified goniometer. The angle of deflection was converted into pressures by the following relation:

$$P = \frac{2D\theta}{\Sigma\, q_i\, A_i\, f_i} \qquad (g)$$

where θ is the angle of deflection, q_i is the distance from the center of orifice i to the axis of cell rotation, A_i is the area of orifice i, and f_i is the correction factor for the nonideality of orifice i.[40,41] D is the torsion constant of the suspension system which is calculated from

$$D = \frac{4\pi^2\,(I_1 - I_2)}{t_2^2 - t_1^2} \qquad (h)$$

where I_1 and I_2 are moments of inertia of two different calibration discs and t_1 and t_2 are periods of rotational oscillation associated with each disc.

To ensure that no extraneous leaks contributed to the measured torque on the cell, assemblies which contained zinc samples but in which no orifices were drilled were heated to temperatures of 620°K. No significant deflection was found.

C. Temperature Measurement

The temperature profile of the furnace in the range 500° to 700°K was very poor, the region in which the temperature was constant within 2° being less than 1.5 cm in length. In order to improve and lengthen the constant temperature region, a 7.5 cm diameter cylinder fabricated of 6 mil copper was placed between the torsion cell and the tungsten hairpins. This arrangement provided a 5 cm zone in which the temperature was constant within 2°.

The temperature of a torsion cell placed in the middle of the constant temperature zone was plotted against the temperature of a chromel-alumel probe thermocouple placed just below the cell to obtain a calibration curve. Temperatures of the cell during the runs were obtained by correcting the measured temperature of the probe thermocouple with the calibration curve. The calibration curve was checked periodically throughout the investigation, and no significant change in the curve was ever noticed. The difference in temperature between the cell and the dummy thermocouple ranged from +5° at 330°K to a -4° at 670°K.

The thermocouples were calibrated by measurements of the melting points of lead and tin.

D. Sample Preparation

Crystals were grown under argon in graphite molds by the well known Bridgeman technique. A rate of 1.3 cm/hr was used. The crystals were formed as rods 3/8" in diameter with the rod axis coincident with the growth axis and with the plane of interest perpendicular to the growth axis.

A single crystal rod purchased from Semi-Elements Inc. was also used in this investigation. Their crystal was a 1/2" diameter rod grown by the Bridgeman technique in a pyrex mold with the rod axis perpendicular to the basal plane. Because rods grown in pyrex molds are susceptible to surface pitting, the rod was acid machined to a 3/8" diameter.

Spectrographic analyses of zinc samples used in this investigation are given in Table I. The commercially purchased zinc will be referred to as high purity zinc since the most obvious difference between the two types is that the commercial crystal was much purer.

Most of the free surface sublimation studies were made with the basal plane of zinc. The crystal rods were annealed in vacuum at a temperature of 350°C for one hour. Rods were cleaved at liquid nitrogen temperatures. Cleavage deformation was minimized by cleaving thin wafers from a large rod until a smooth surface was obtained on the bulk rod. Then a wafer about 5 mm thick was cleaved from the rod and used in the free surface sublimation runs. This technique enabled most of the cleavage deformation to be absorbed by the thin wafers and not the surface of the bulk rod which eventually became the surface of study.

To reduce contamination from water condensation on the surface, the cleaved crystal was transferred to a methyl alcohol bath in a glove box that had been flushed with and bathed in argon. The crystal was kept in the methyl alcohol until it warmed to room temperature, was dried in a stream of air, and was stored in a dessicator until used.

Table I. Spectrographic analysis of zinc samples

element	bulk zinc	grown crystal	purchased crystal
zinc		principal constituent	
iron	.0050%	---	---
copper	.0005%	.0008%	---
silver	.0005%	.0005%	---

A number of experiments were carried out on the $(10\bar{1}0)$ plane. The prismatic surface was prepared by first growing a crystal oriented with the prismatic plane perpendicular to the rod axis. Then cuts perpendicular to the rod axis were made with a spark cutter, giving wafers of about 5 mm thick. The surfaces were mechanically polished with paper of Nos. 0, 00, 000, and 0000. The final polish was performed with a polishing solution of 1μ alumina suspended in kerosene. Polished samples were rinsed in acetone, and stored in a dessicator until used.

E. Dislocation Density Measurement

Dislocation densities and position intersecting the basal plane were determined using the etch pit technique. A solution of .5M HBr in ethanol, which was shown by Rosenbaum and Saffren[33] to be a suitable etchant, was used in this investigation. The usual etching procedure was to dip the crystal into the etchant with the surface of interest facing upward. After the etching period which was about 5 seconds, the sample was washed in ethanol and dried in a stream of air.

III. KNUDSEN EFFUSION RESULTS AND DISCUSSION

Measurement by different investigators even for an unreactive metal such as silver have yielded a variety of different pressure versus temperature curves.[42-44] Therefore, a comparison of free surface pressures collected in one laboratory with equilibrium pressures measured in another cannot be trusted to yield reliable evaporation coefficients. Accordingly, the equilibrium pressure of zinc was determined as a function of temperature as a check on the experimental apparatus and technique, and to ensure against serious systematic error.

Knudsen effusion data were collected in the range 510° to 690°K. The orifice dimensions are listed in Table II. A variety of combinations of orifice areas and torsion wire diameters was used in order to extend the range of pressures from 10^{-4} to 10^{-7} atm and still maintain a large and stable angle of deflection. The zinc used for the effusion runs were chips of the crystals used for the free surface sublimation runs. Data were collected only after 10% or more of the zinc had been sublimed by heating at about 625°K for 10 minutes. Knudsen effusion runs were made with zinc from the grown crystal and from the high purity crystal.

The data are presented in Table III and Fig. 5. As seen in Fig. 5, there was no distinguishable difference in equilibrium pressures measured for zinc from the two different sources. At least squares fit of the data yields an equation of

$$\log P_{atm} = -(6.683 \pm .095)\frac{10^3}{T} + 5.893 \pm (.029) \qquad (1)$$

The equation is represented by the dotted line of Fig. 5. Using the

Table II. Orifice dimensions

type of experiment	orifice diameter (cm)	channel length (cm)	force correction factor
Knudsen-effusion	.2376	.1549	.6746
	.2365	.1575	.6704
	.0992	.1643	.4476
	.0988	.1279	.5034
	.3050	.1532	.7319
	.3050	.1534	.7315
	.2540	.1499	.6975
	.2542	.1515	.6952
torsion-Langmuir	.3056	.1080	.7983
	.3068	.1147	.7476
	.3600	.1157	.8139
	.5236	.1163	.8634
	.5234	.1234	.8585

Table III. Equilibrium vapor pressure of zinc

orifice diameter (cm)	wire size (mil)	temp. (°K)	press. (atm)	orifice diameter (cm)	wire size (mil)	temp. (°K)	press. (atm)
.2376	2.0	641	2.643×10^{-5}	.2376	1.5	570	1.608×10^{-6}
.2365		578	2.320×10^{-6}	.2365		595	5.124×10^{-6}
		593	4.820×10^{-6}			573	1.895×10^{-6}
		609	8.520×10^{-6}			583	3.072×10^{-6}
		630	2.005×10^{-5}			586	3.432×10^{-6}
		635	2.488×10^{-5}			571	1.529×10^{-6}
		638	2.865×10^{-5}			592	4.482×10^{-6}
		604	7.001×10^{-6}			563	1.090×10^{-6}
		628	2.032×10^{-5}				
		616	1.115×10^{-5}	.2376	1.0	515	8.620×10^{-8}
		597	5.132×10^{-6}	.2365		533	2.093×10^{-7}
		627	1.805×10^{-5}			547	4.795×10^{-7}
		597	5.320×10^{-6}			543	3.223×10^{-7}
						557	7.686×10^{-7}
.099	2.0	600	6.064×10^{-6}			523	1.423×10^{-7}
.099		637	2.928×10^{-5}			548	5.078×10^{-7}
		638	2.470×10^{-5}			519	1.096×10^{-7}
		657	6.070×10^{-5}			533	2.627×10^{-7}
		677	1.071×10^{-4}			519	1.099×10^{-7}
		683	1.419×10^{-4}			535	3.069×10^{-7}
		664	7.641×10^{-5}			553	7.072×10^{-7}
						554	7.355×10^{-7}
.3050	1.5	570	1.488×10^{-6}			569	1.465×10^{-6}
.3050		565	1.164×10^{-6}			518	1.009×10^{-7}
		552	6.402×10^{-7}			528	1.883×10^{-7}
		542	4.009×10^{-7}			519	1.101×10^{-7}
		533	2.564×10^{-7}			519	1.005×10^{-7}
						527	2.160×10^{-7}
.2540	1.5	557	9.949×10^{-7}			549	5.117×10^{-7}
.2542		571	1.795×10^{-6}			536	2.732×10^{-7}
		588	3.704×10^{-6}			538	3.118×10^{-7}
		604	7.224×10^{-6}			525	1.636×10^{-7}
		611	1.049×10^{-6}			539	3.301×10^{-7}
		593	4.402×10^{-6}			523	1.526×10^{-7}
		567	1.308×10^{-6}			522	1.532×10^{-7}
		548	5.072×10^{-6}			534	2.518×10^{-7}
						532	1.904×10^{-7}
						550	5.419×10^{-7}
			purchased zinc				
.2540	1.5	578	2.401×10^{-6}			576	2.137×10^{-6}
.2542		600	5.841×10^{-6}			585	3.110×10^{-6}
		550	6.231×10^{-7}				

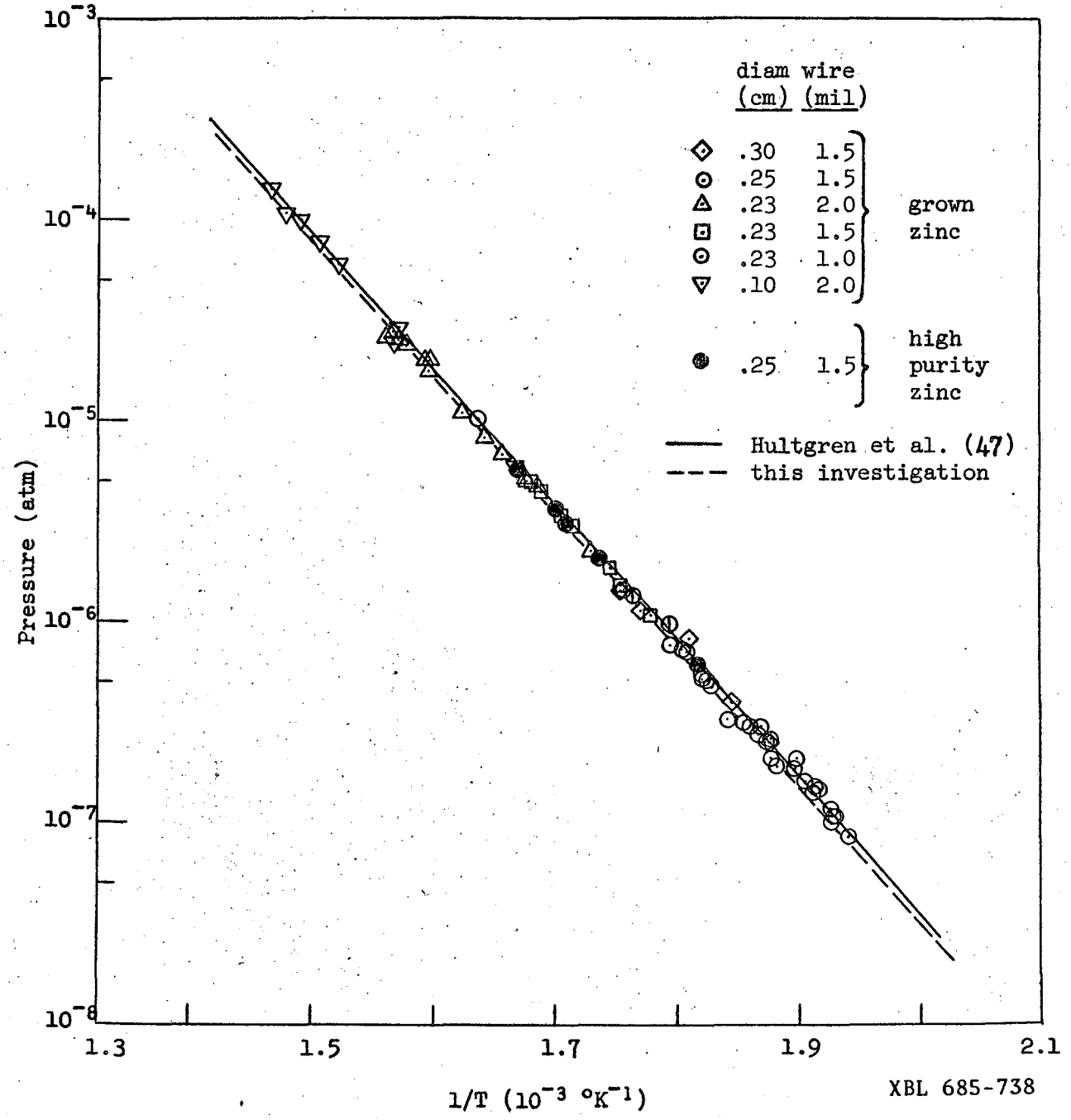

Fig. 5. Knudsen effusion results for zinc.

free energy functions tabulated by Stull and Sinke,[45] the average third law heat of sublimation is calculated to be $\Delta H^{\circ}_{298} = 31.294 \pm .075$ as compared to $\Delta H^{\circ}_{298} = 31.245 \pm .050$, reported by Hultgren, Orr, Anderson, and Kelly[46] from a critical evaluation of 15 different experimental studies.

As seen from Fig. 5, the equilibrium data collected in this investigation are in excellent agreement with the values accepted by Hultgren et al. The difference at 540°K expressed as a difference in the third law heat of sublimation is only 0.2%. This difference, however, if uncorrected would produce an 8% error in the value reported for α.

IV. STEADY STATE FREE SURFACE SUBLIMATION

A. Evaporation Coefficient Measurements

The free surface sublimation pressures are presented in Table IV and plotted on Fig. 6. The solid line represents the equilibrium data collected in this investigation. Table IV also contains values of α calculated from the ratio of each free surface pressure to the equilibrium pressure given by Eq. (i).

The evaporation coefficients measured from the (0001) surface of the high purity zinc averaged 1.1 ± .08. The evaporation coefficient for the $(10\bar{1}0)$ surface of the grown zinc averaged 1.02 ± .09. In contrast, the evaporation coefficient for the (0001) surface of the grown zinc averaged .73 ± .08. All uncertainties listed are standard deviations from the mean.

Langmuir data from different planes, different crystal sources, and Knudsen data were collected interchangeably throughout most of this investigation; therefore, the marked difference in behavior of the (0001) plane of the grown zinc from that of the $(10\bar{1}0)$ plane of the grown crystals and from (0001) planes of the high purity crystals appeared to be real. Conclusive proof that α was different for the (0001) plane of the grown crystal was obtained by the use of a differential torsion cell which had two sets of orifices arranged so that the torque produced by vaporization from one pair of surfaces opposed the torque produced by evaporation from the others. The differential torque from the (0001) and $(10\bar{1}0)$ surfaces was measured. By proper combinations of orifice area, wire constant, and temperature, deflection angles of 5 - 40° were

Table IV. Free surface sublimation results

surface	temperature (°K)	pressure (atm)	α
(0001) high purity zinc	574	1.915×10^{-6}	1.08
	656	7.847×10^{-7}	1.13
	591	3.981×10^{-6}	1.06
	574	1.967×10^{-6}	1.10
	558	9.605×10^{-7}	1.24
	583	2.676×10^{-6}	1.01
	593	4.067×10^{-6}	.99
	595	4.370×10^{-6}	.98
	546	5.528×10^{-7}	1.29
	530	2.422×10^{-7}	1.21
(0001) grown zinc	604	5.122×10^{-6}	.74
	629	1.511×10^{-5}	.79
	630	1.539×10^{-5}	.56
	578	1.896×10^{-6}	.87
	621	1.109×10^{-5}	.80
	557	1.783×10^{-6}	.85
	558	5.666×10^{-7}	.68
	556	5.149×10^{-7}	.66
	564	8.585×10^{-7}	.75
	546	3.173×10^{-7}	.70
	564	8.999×10^{-7}	.78
	537	2.397×10^{-7}	.81
	531	1.870×10^{-7}	.88
	556	4.814×10^{-7}	.64
	539	2.352×10^{-7}	.74
	560	6.350×10^{-7}	.67
	573	1.264×10^{-6}	.76
	576	1.333×10^{-6}	.69
	572	1.282×10^{-6}	.79
	575	1.240×10^{-6}	.65
	573	1.141×10^{-6}	.69
	575	1.274×10^{-6}	.67
	571	1.011×10^{-6}	.67
	575	1.097×10^{-6}	.57
	517	6.690×10^{-8}	.70
	516	7.797×10^{-8}	.85
	535	1.670×10^{-7}	.67
	563	8.577×10^{-7}	.78
	637	2.298×10^{-7}	.76

Table IV. continued

surface	temperature (°K)	pressure (atm)	α
$(10\bar{1}0)$			
grown zinc	570	1.472×10^{-6}	1.02
	611	9.997×10^{-6}	1.07
	529	1.952×10^{-7}	1.02
	534	2.293×10^{-7}	.96
	532	2.189×10^{-7}	1.00
	585	2.635×10^{-6}	.90
	589	3.890×10^{-6}	1.23
	543	4.110×10^{-7}	1.06

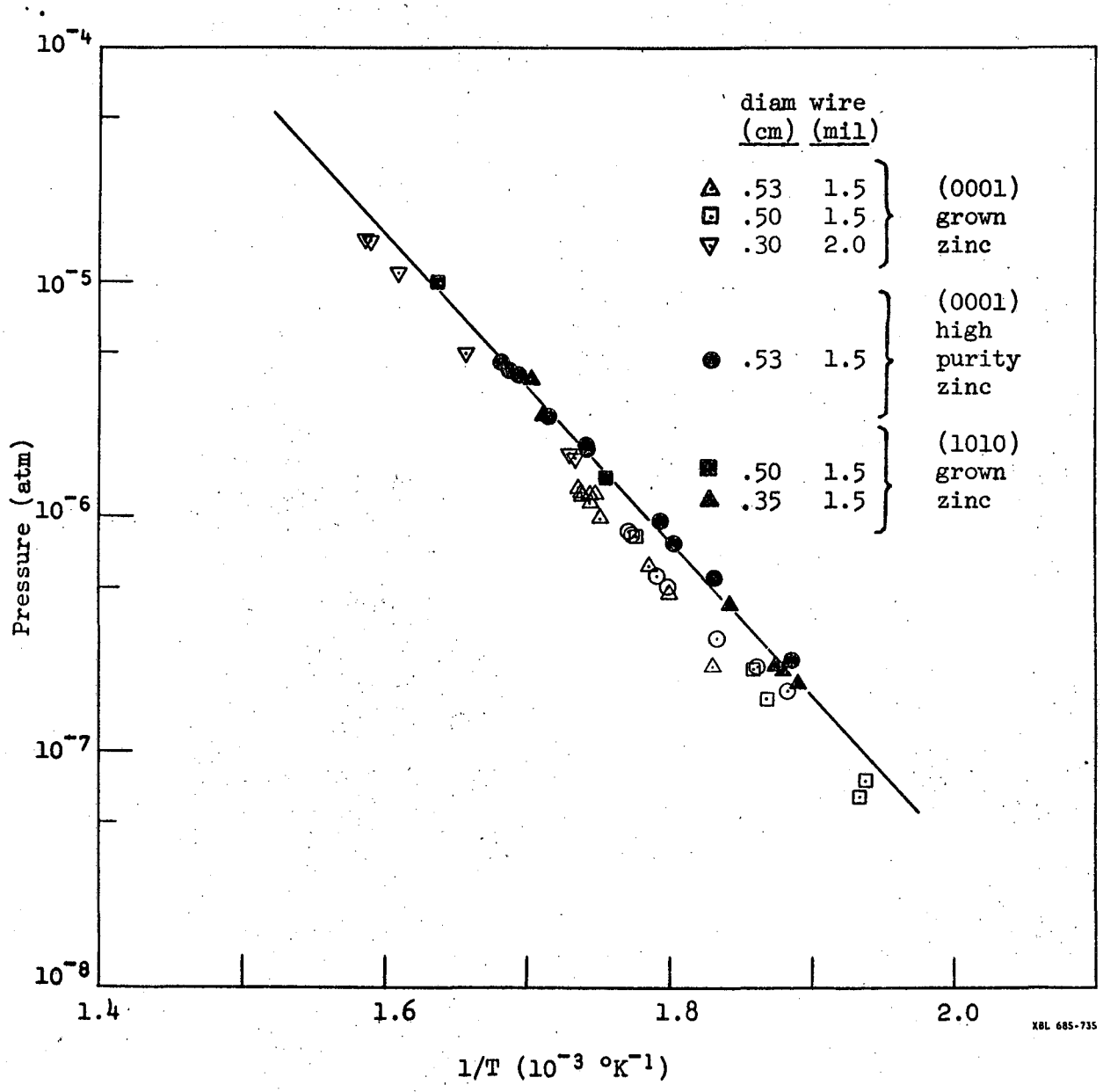

Fig. 6. Free surface sublimation results for zinc.

obtained. To protect against the possibility that the direction of orifice orientation or orifice dimensions might cause a significant differential torque, the crystals were interchanged and the measurements were repeated. The orifice dimensions are shown in Table V. The data are collected on Table VI.

If one accepts Eq. (i) as the pressure for the $(10\bar{1}0)$ surface, then the basal plane is calculated to have an average evaporation coefficient of $0.71 \pm .04$ from these differential runs. This is in excellent agreement with the value of $0.73 \pm .08$ as calculated from the absolute Langmuir runs.

B. Chemical Etch Pit Measurements

The experimental evaporation coefficients for the low index crystal faces studied were clearly higher for all crystals and planes studied than the value of 1/3 predicted by the Hirth and Pound theory for perfect, low index crystal surfaces.[11,12] But the theory predicts that α will be greater than 1/3 for surfaces which are intersected by a high concentration of screw dislocations. High, but different dislocation densities in the grown and high purity zinc crystals might explain the high, but different values of α which were measured for the crystals from the different sources. Accordingly, chemical etching was performed by the methods developed by Rosenbaum and Saffren[33] and previously used by Ruff.[35]

Chemical etch pit counts were made for six samples of grown zinc and three of high purity zinc. Counts ranged from 3.6×10^4 pits/cm^2 on the most imperfection-free surface to 2.1×10^5 pits/cm^2 on the most imperfect surface. Some samples displayed high and low etch pit density regions on the same surface, with densities varying from 9.2×10^3 to

Table V. Orifice dimensions used in differential cell

set*	orifice diameter (cm)	channel length (cm)	force correction factor	fA**	fA
A	.5236	.1163	.8634	.1859	.3716
	.4862	knife edged	1.0000	.1857	
B	.5234	.1234	.8565	.1848	.3717
	.4883	knife edged	1.0000	.1869	

*set A was opposed to set B

**fA = (force correction factor)(orifice area)

Table VI. Differential torsion cell results

temperature (°K)	$\Delta\theta$* (deg)	Δ pressure (atm)	$\alpha_{(0001)}$**
572	15.155	$.62 \times 10^{-6}$	.62
569	14.100	$.57 \times 10^{-6}$	.67
570	13.803	$.55 \times 10^{-6}$	.68
589	18.720	$.94 \times 10^{-6}$	.73
610	38.725	$.20 \times 10^{-5}$	.77
589	12.760	$.64 \times 10^{-6}$	.73
557	4.547	$.23 \times 10^{-6}$	.70
582	12.845	$.65 \times 10^{-6}$	.74
554	3.690	$.19 \times 10^{-6}$	.73

* + if $(10\bar{1}0)$ torque > (0001) torque

\- if $(10\bar{1}0)$ torque < (0001) torque

** based on the assumption that $\alpha_{(10\bar{1}0)} = 1$

6.0×10^5 pits/cm^2. Fortunately, the high density areas were usually confined to visibly distorted areas near the edges of the crystal, and the area defined by the orifice could be chosen from the more perfect center portion of the crystal. No consistent differences in the dislocation densities between grown and high purity zinc were found.

C. Morphology of Surfaces During Steady State Sublimation

Because the kinetics of sublimation reactions may well be closely correlated with the surface structure, the morphology of the various surfaces were examined at various magnifications with an optical microscope and with a scanning electron microscope. The (0001) surfaces of the grown and high purity zinc were distinctly different from each other and from the $(10\bar{1}0)$ surface.

The (0001) surface of the high purity zinc looked like a flat plain with a number of interconnecting ridges. Two typical surfaces at apparently different stages of development are shown in Fig. 7. The features varied slightly from sample to sample. On some, the ridges met the flat portions along definite curved lines as on Fig. 8-b, and on others there was a smooth transition from the ridge to the plain (Fig. 8-a).

A typical (0001) surface of the grown zinc showed broad macroscopic pits on a relatively flat surface (Fig. 9). The largest pits were on the order of 700μ in diameter and the depth of the pits ranged from 100μ to ones just starting. Some surfaces were completely free of the large pits and the entire surface resembled the flat area between the pits on Fig. 9. This type of surface is shown on Fig. 10-a. Figures 10-a through 10-f show successive stages of surface development. Upon

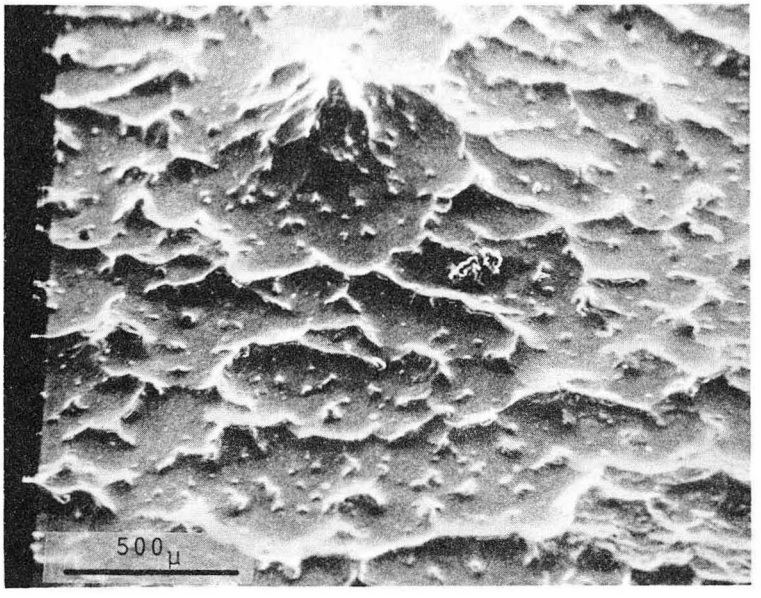

(a)

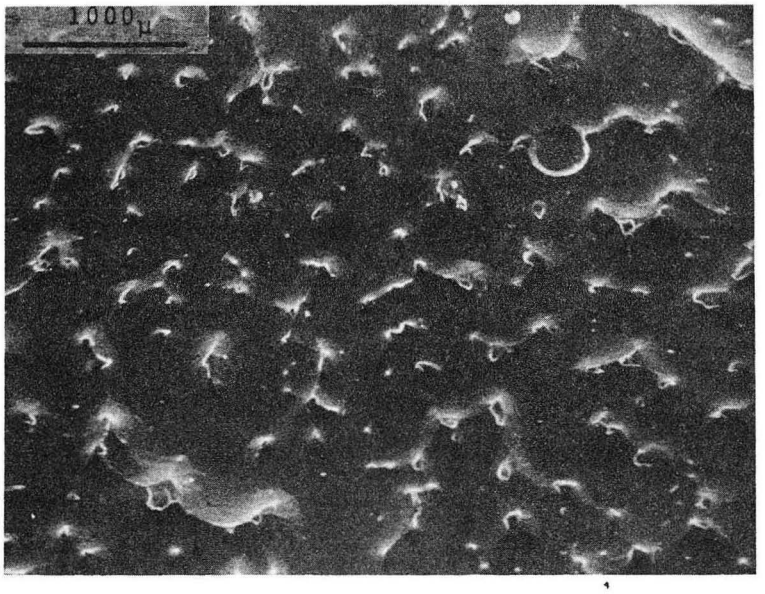

(b)

XBB 687-4160

Fig. 7. (0001) surface after evaporation from different samples of high purity zinc.

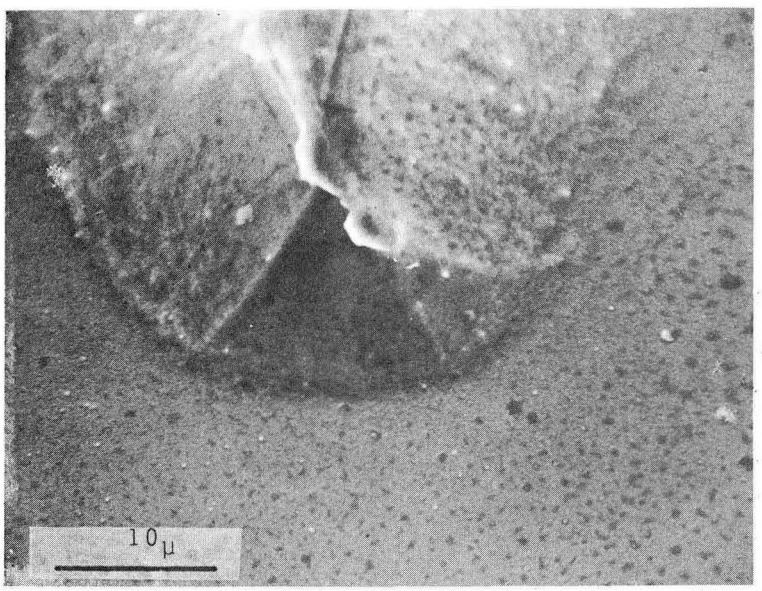

(a)

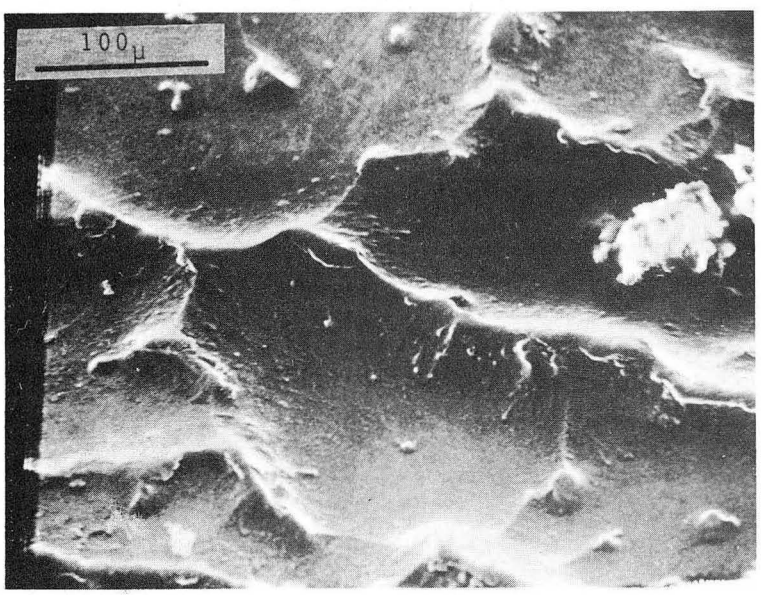

(b) XBB 687-4161

Fig. 8. Ridge features on (0001) surface of high purity zinc.

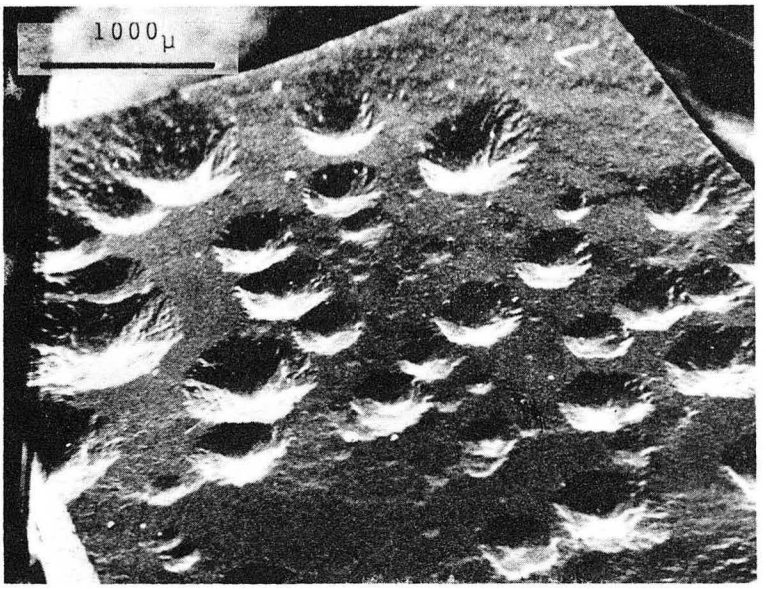

XBB 687-4162

Fig. 9 Typical (0001) surface of grown zinc after evaporation.

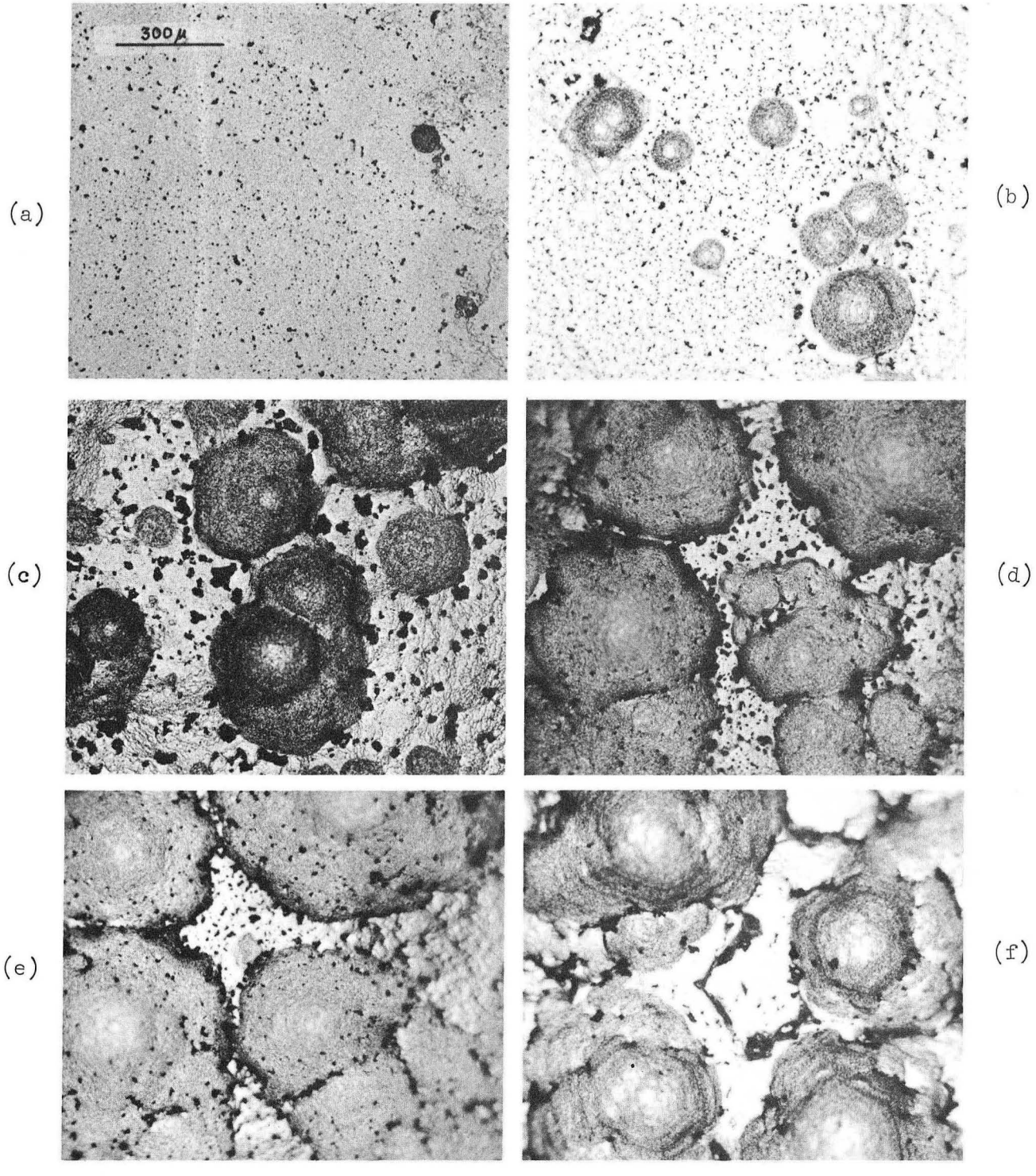

XBB 685-2681

Fig. 10 Development of (0001) surface of grown zinc during steady state sublimation.

further sublimation the surface of Fig. 10-a started to develop pits. Throughout the sublimation, a number of small pits of the kind seen on Figs. 9 and 10-a were formed, but only a few pits ever reached macroscopic sizes. As seen from comparison of Fig. 10-f to 10-e, when the walls of the pits touched, a new plateau surface began to spread at the expense of the previously spreading pits.

The macroscopic pits were flat bottomed (Fig. 11) and the sides were composed of a number of very closely spaced ledges (Fig. 12-a). Figure 12-b shows the ledges which characterize each of the six sides of the hexagonal pit walls, and Fig. 12-c shows one of the areas in which ledges of two such wall sections meet. The steady state pressures showed no measureable variations during these changes in surface structure.

An examination of the flat area between the large pits showed some portions to be very flat (Fig. 13-a), with no relief visible at magnifications as high as 30,000X except for rather randomly spaced small hexagonal pits. Other areas were composed of widely spaced ledges (Fig. 13-b).

Small hexagonal pits (see Figs. 11, 12, and 13) formed on the flat areas between pits, the flat bottoms of the large pits, and the steep sides of the pits. Pit densities ranged from 1.1×10^7 pits/cm^2 in the densest areas to 3.0×10^6 in the sparsely populated areas. Diameters of these pits were on the order of 1-3μ. Whatever the cause of these small pits, they were usually ineffective in altering the ledge motion as it is seen that the ledges develop as if the pits were not there.

The pits from which the macroscopic pits developed were examined

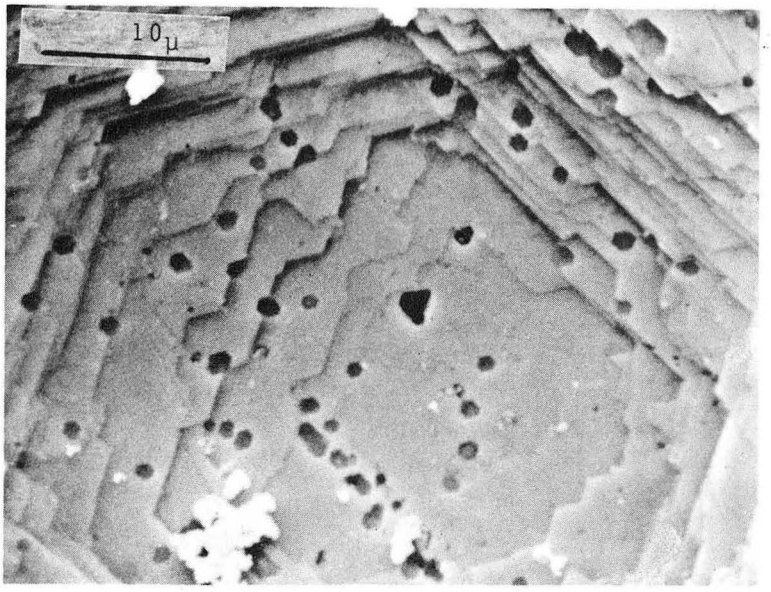

XBB 687-4163

Fig. 11 Flat bottom of one of the macroscopic pits of Fig. 9.

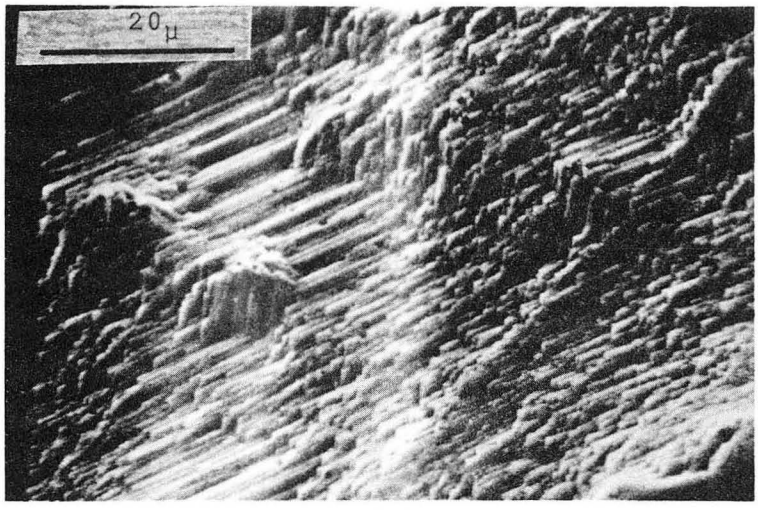

(a)

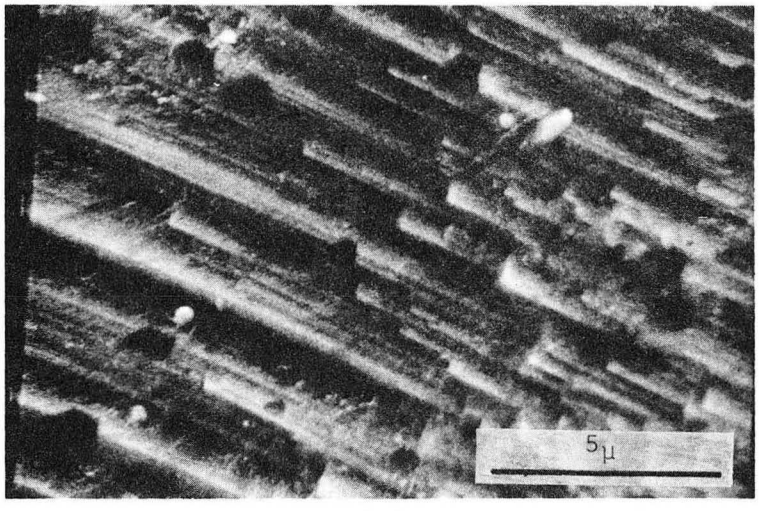

(b)

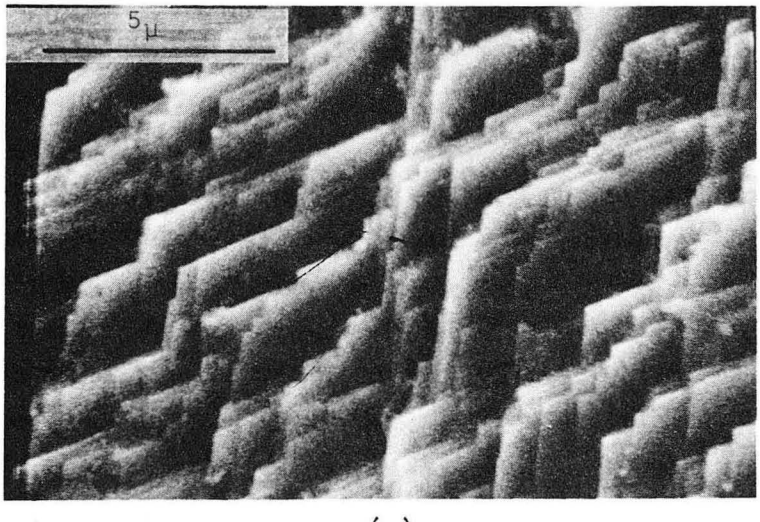

(c)

XBB 687-4164

Fig. 12 Ledged structure on the side of the macroscopic pit.

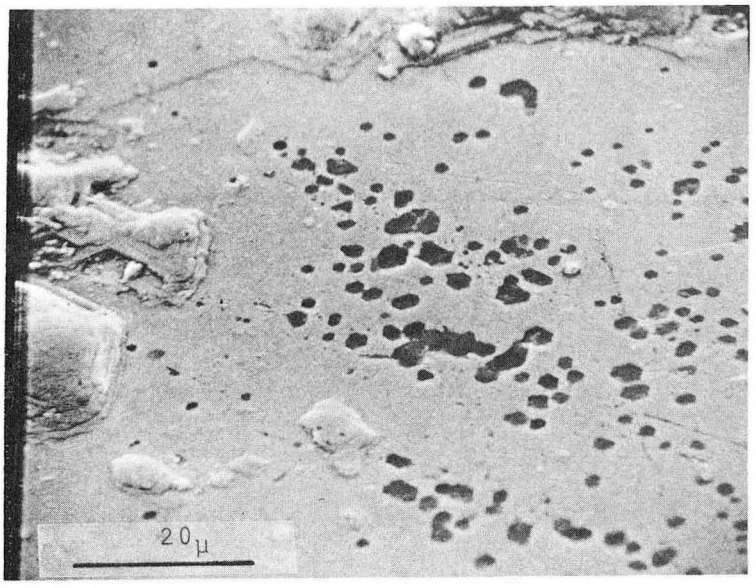

(a)

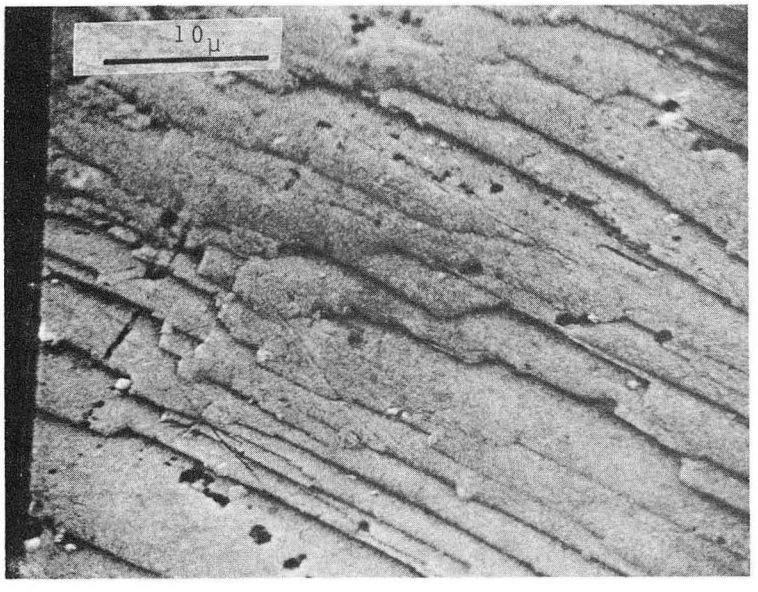

(b) XBB 687-4165

Fig. 13 Flat (0001) surface between macroscopic pits of Fig. 9.

at higher magnifications. It was found that these starting pits had tiered walls that steepened with depth and appeared to emanate from one of the small hexagonal pits just discussed. Figure 14 illustrates this point quite clearly. These steep sided pits eventually developed flat bottoms of the type shown on Fig. 11. These successive stages of pit development are clearly illustrated in Fig. 15 where the three pits on the left are still actively deepening and the pit on the right is flattened on the bottom. A large macroscopic pit developed only if the penetration depth was large before the pit started to flatten at the bottom. It is apparent from Fig. 14 that the presence of one of the 1-3μ hexagonal pits is a necessary condition for initiation of growth of a macroscopic pit. But for reasons that are not apparent from surface examination, only a small fraction of the small pits act as sites for initiation of macroscopic ledges.

The surface features on the $(10\bar{1}0)$ planes were quite complex. The surface was characterized by a vast array of crystallographic peaks and striations. Micrographs of a surface at various magnifications are shown on Fig. 16. Figures 16-a and 16-b show different stages of development. The ledge striations are predominantly in one direction; however, Fig. 16-c shows that the ribbed features consist of ledges perpendicular to the direction of the major striations.

Throughout any period of the steady state, particles that appeared dark in the optical micrographs and light in the electron micrographs could be seen to grow on the surface. The particles were like flaky, loose growths from the surface. While the particles formed in patches

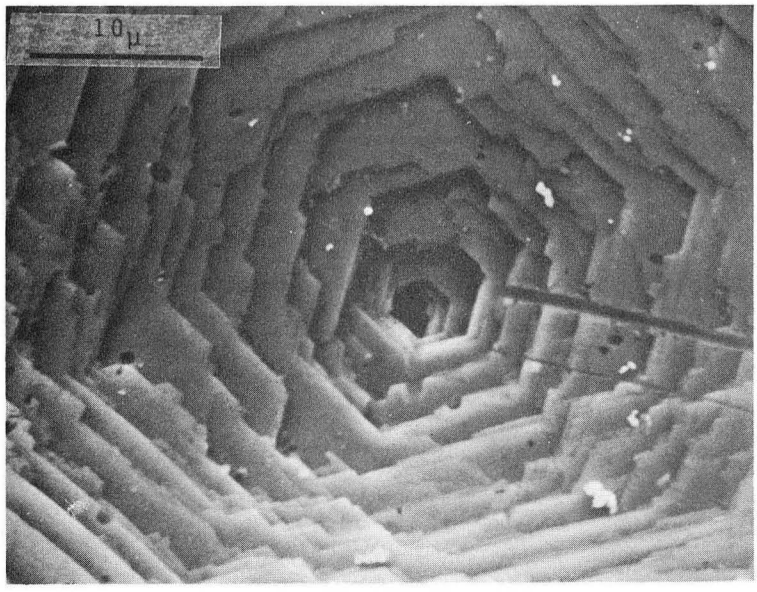

(a)

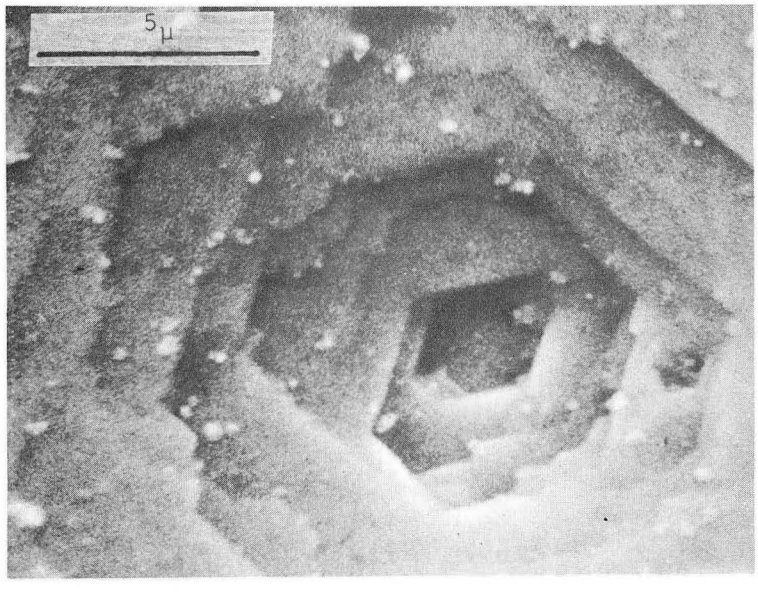

(b) XBB 687-4166

Fig. 14 Pits starting in the (0001) surface of the grown zinc which eventually developed into macroscopic pits.

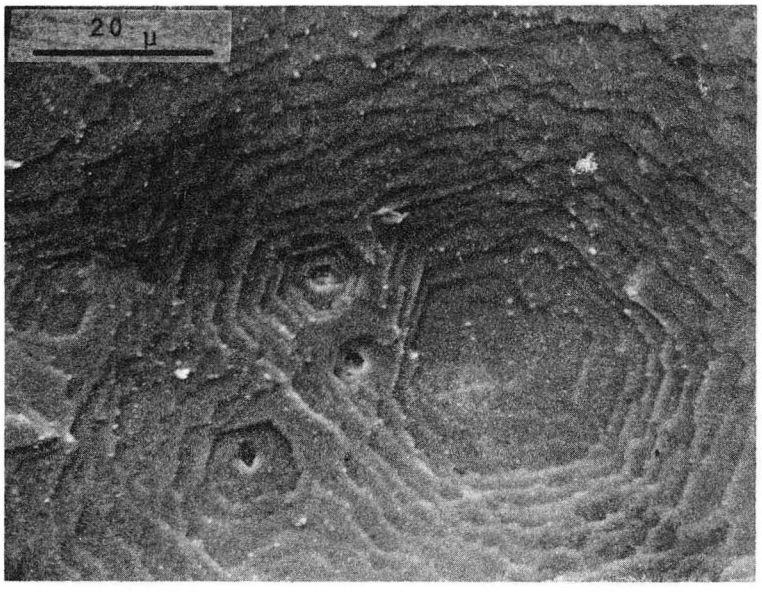

XBB 687-4167

Fig. 15 Pits in the (0001) surface of grown zinc at different stages of development.

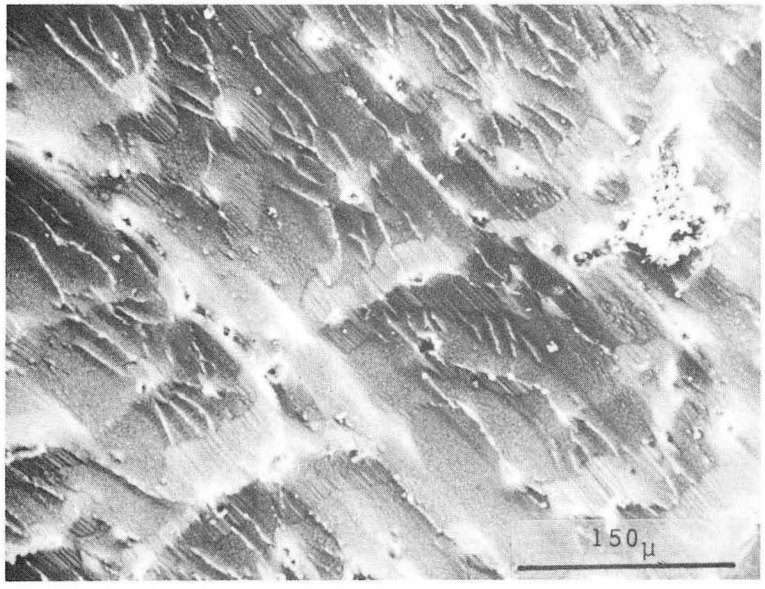

(a)

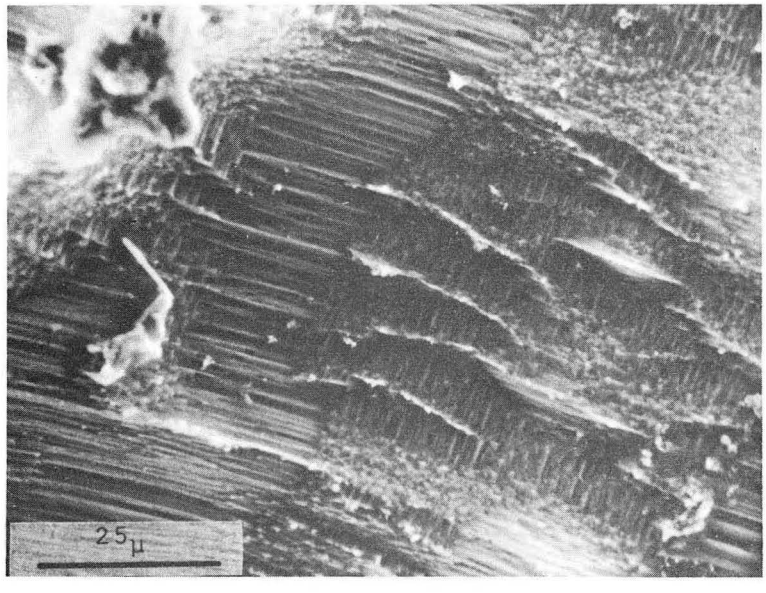

(b)

XBB 685-3105

Fig. 16 Surface development on the (10l0) surface of the grown zinc.

and along ledges on the grown zinc, they were mainly congregated along the ridges of the high purity zinc. These particles congregated at the tops of the peaks on the $(10\bar{1}0)$ surfaces.

Ledge motion in the growth of macroscopic pits is hindered by these particles (Fig. 17). Many of the particles were remarkably mobile and it is seen on Fig. 10 that they were pulled along by the prismatic side faces of growing pits.

The particles were very loosely held on non-pitted surface regions. A stream of air was sufficient to remove most of them. Figure 13-a shows raised areas upon which these particles resided before they were dislodged during the sample preparation treatment for the scanning electron microscope. The raised areas formed because sublimation was impeded under the particles.

The particles were not clearly seen on the electron micrographs of the high purity surfaces because they were for the most part removed during the preparation for the electron microscope. Through the use of an optical microscope prior to the preparation, the white ridge areas of Fig. 7 were established as the surface regions where the particles collected and masked sublimation of the zinc.

Since the crystals were grown in graphite molds and graphite torsion cells were used, the possibility that the particles were carbon was considered. A microprobe analysis of the particles gave no indication that they contained carbon or measurable amounts of metallic elements other than zinc. However, the microprobe analysis is not conclusive because it is relatively insensitive for carbon analysis and is not well

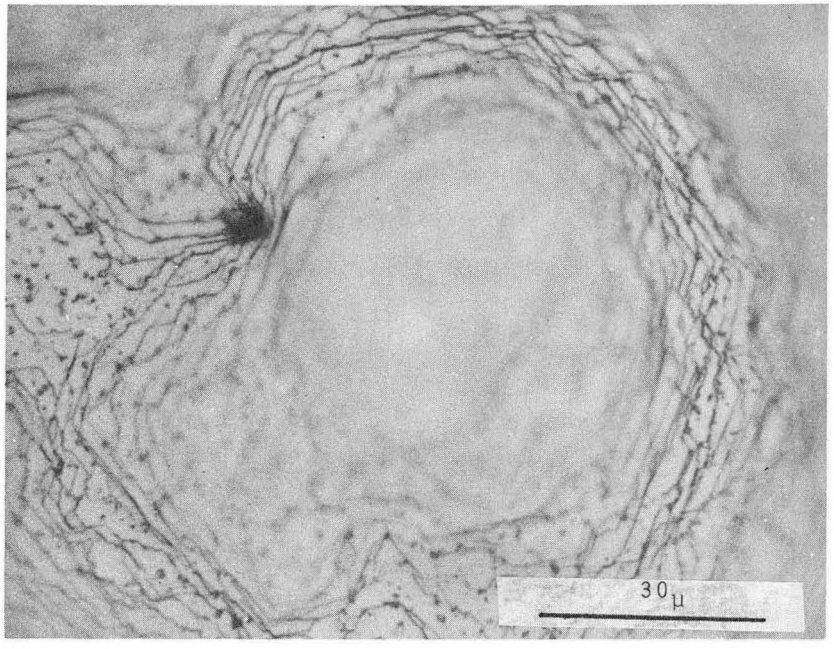

XBB 687-4168

Fig. 17 Interaction between evaporation ledges and a second phase particle on the (0001) surface of grown zinc.

suited to analyzing rough surfaces. It was found by experiment that samples grown in quartz molds and samples sublimed in alumina cells with alumina orifices developed the same surface particles.

The particles are thought to be ZnO, produced by the reaction

$$Zn(s) + 1/2O_2(g) \rightarrow ZnO(s).$$

Using the thermochemical data for Zn(s), $O_2(g)$ and ZnO(s) as tabulated by Kubaschewski, Evans and Alcock,[47] the free energy of this reaction was calculated at temperatures ranging from 470° - 690°K. The free energy of reaction was highly negative at all temperatures. At 575°K oxygen partial pressures less than 10^{-50}atm are needed to prevent the reaction, while during this investigation the total pressure was on the order of 10^{-7} torr.

Surfaces sublimed for very long times accumulated large amounts of the particles. An x-ray diffraction pattern was obtained from one such surface. In addition to the principal lines for the basal surface of zinc there were a few extra lines. Spacings of the extra lines corresponded with spacings expected for ZnO, but their relative intensities did not correspond with the relative intensities expected for randomly oriented ZnO. This fact does not negate the possibility that ZnO was formed for one would expect that ZnO, if formed, would be strongly oriented. The two strongest lines observed corresponded to the (202) and (101) planes of ZnO.

The volume of particles formed on the surface was less dependent on temperature than was the zinc sublimation rate. A surface held at

about 470°K for more than twelve hours was heavily laden with the particles although the surface recession due to evaporation was relatively small. A sample evaporated at about 620°K for less than 70 minutes underwent greater surface recession, but showed considerably less particle formation.

This temperature dependence is reasonable if these particles were ZnO formed by the oxidation of zinc, because, for oxidation, the rate may be determined primarily by the rate at which oxygen is supplied to the surface. The temperature dependence is not consistent with the assumption that the particles are impurities from the zinc. For impurities to collect at the surface at a rate faster than the surface receded would require that the impurities, which are at concentrations well below their solubility limits, must diffuse out and precipitate as a new phase. Such behavior would seem thermodynamically impossible.

Scanning electron micrographs (Fig. 18) shows the structure of the particles on the heavily laden surface at various magnifications. The behavior of the particles in the electron beam was very interesting. Occasionally a portion of a particle shifted as the beam passed over it. This might have been due to the fact that Zn rich ZnO is not a good enough conductor at high beam voltages to prevent some electrostatic charging, so that adjacent particles repelled each other. It was difficult to maintain the focus on the particles at high magnifications. The difficulty may have been caused by motions of parts of the loosely held and fluffy particles relative to other parts as a result of variations in charges.

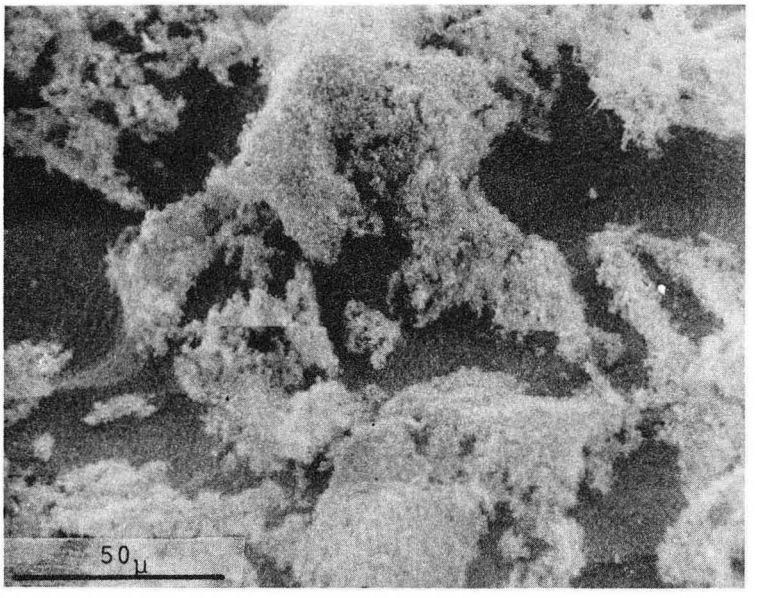

(a)

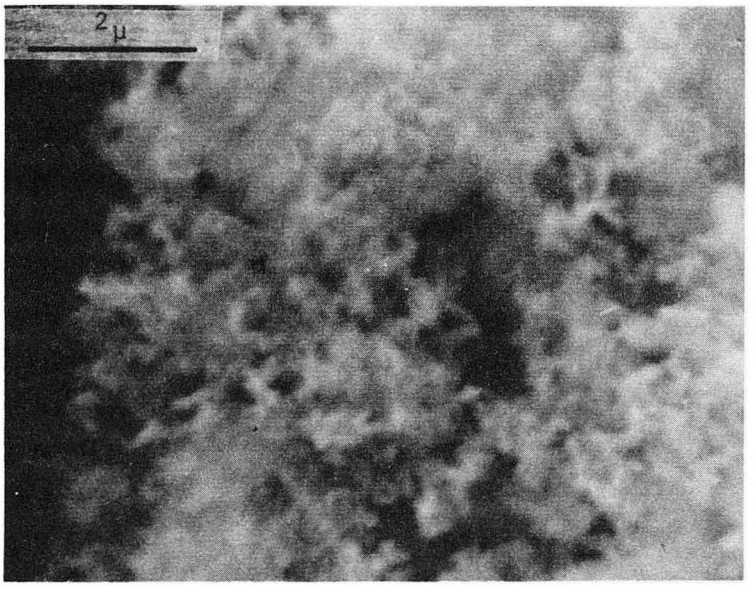

(b)

XBB 687-4169

Fig. 18 Structure of zinc oxide particles formed on a purposely heavily laden (0001) surface.

Because zinc oxide should form by reaction of zinc and oxygen at the background pressures in the vacuum chamber, and because all the measured properties of the surface particles are consistent with those expected for zinc oxide, it seems certain that they are zinc oxide.

The oxidation of zinc at higher oxygen pressures has been shown to follow the parabolic law[48-50] or at relatively low temperatures, a logarithmic law.[51,52] It might be expected, therefore, that oxide formation would produce a protective coating that gradually would reduce the measured rate of the zinc sublimation. Observations that, at the low oxygen pressures of this study, the oxide remains in discrete patches provides a partial explanation of why sublimation is not measureably reduced by oxide formation. The sequence of micrographs 10 suggest an explanation of why these patches do not eventually cover so much of the surface that the zinc flux is noticeably reduced. Note that the sizes of particles (black in these optical micrographs) increase in the sequence 10-a to 10-e, but is very small again in 10-f. The particles on the flat surfaces grow with time until the macropit boundaries intersect, annihilating the ledge surfaces to which the particles clung. The particles then probably dropped off the vertically held surfaces.

Hirth and Pound in analyzing the dynamics of ledge motion have shown that crystal edges are very ready sources for evaporation ledges.[11] Accordingly, experiments were performed on sublimation of (0001) surfaces in order to see what differences in surface morphology might result. The surfaces of the grown zinc remained very flat during sublimation. During the course of numerous runs on numerous samples, pits of the sizes

shown on Figs. 9 and 14 never developed. Instead, ledges were seen to be generated at the crystal edges. Occasionally an area would develop a few pits of the type shown on Fig. 10-b, but these pits never achieved macroscopic sizes.

Fig. 19 shows how most of a grown crystal surface looked at various magnifications. There were no ledge features or pits on the relatively smooth surface. The zinc oxide particles formed in randomly spaced little clumps. The surface was flat enough for subgrain reflections to be detected by the naked eye.

A corresponding series of photographs showing the behavior of a zinc sample from a different grown crystal rod and subjected to the same procedure is shown on Fig. 20. The surface was pitted and ledge, although there was once again the absence of large macroscopic pits seen on the orifice defined areas.

High purity zinc samples were also sublimed with the edges exposed. The surface appearance was no different from that of the orifice defined surfaces.

D. Discussion of Steady State Behavior

The surface features on the high purity zinc resembled those observed by Hirth and Winterbottom[28] in their work on silver. Frank's topographical theory[53] has been used in conjunction with the Hirth and Pound theory[11,12] to describe the surface morphology of the silver. Hillocks or ridge formations were attributed to an impurity effect and the shape of the area between hillocks was treated theoretically by the Frank theory of topography.

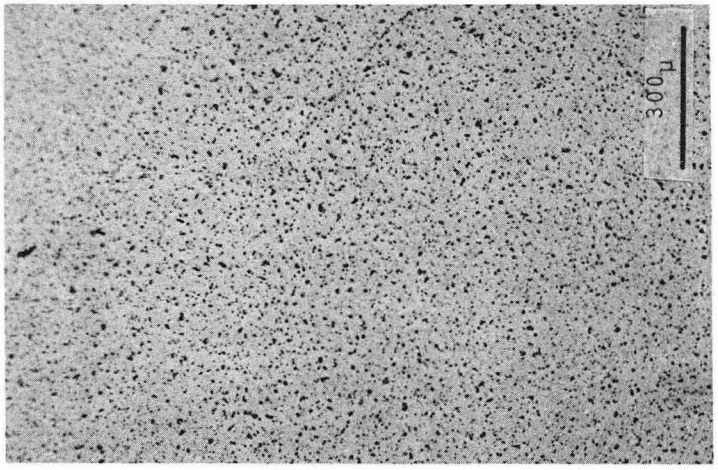

(a)

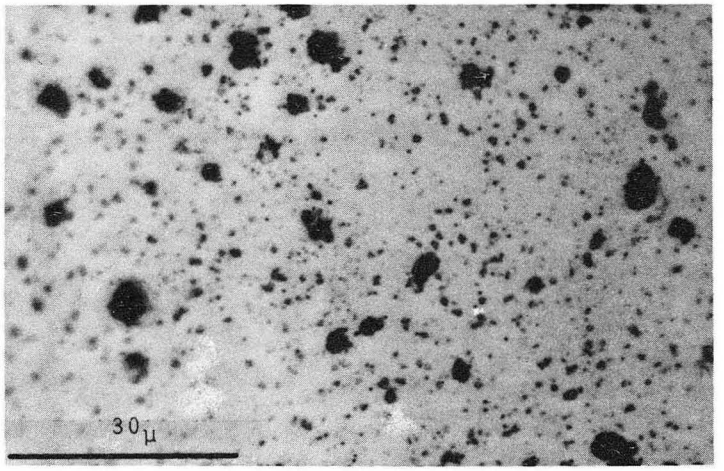

(b)

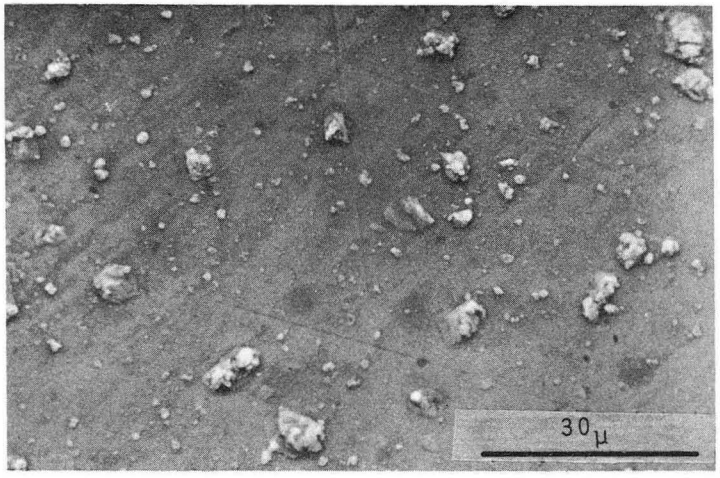

(c)

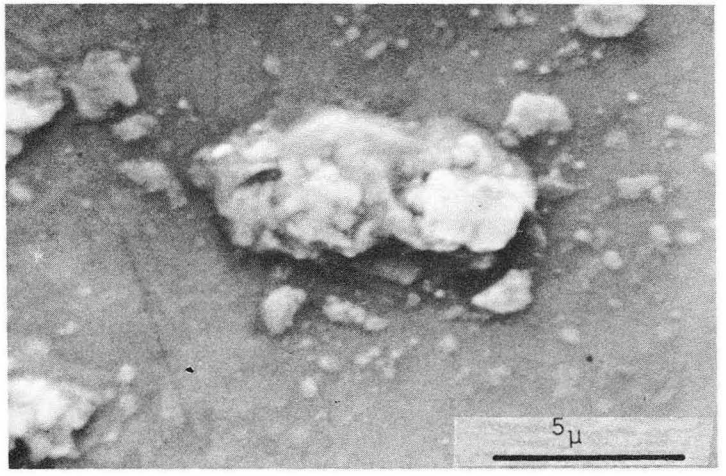

(d)

XBB 687-4170

Fig. 19 (0001) surface of grown zinc which sublimed with crystal edges exposed. (a) and (b) are optical micrographs. (c) and (d) are electron micrographs.

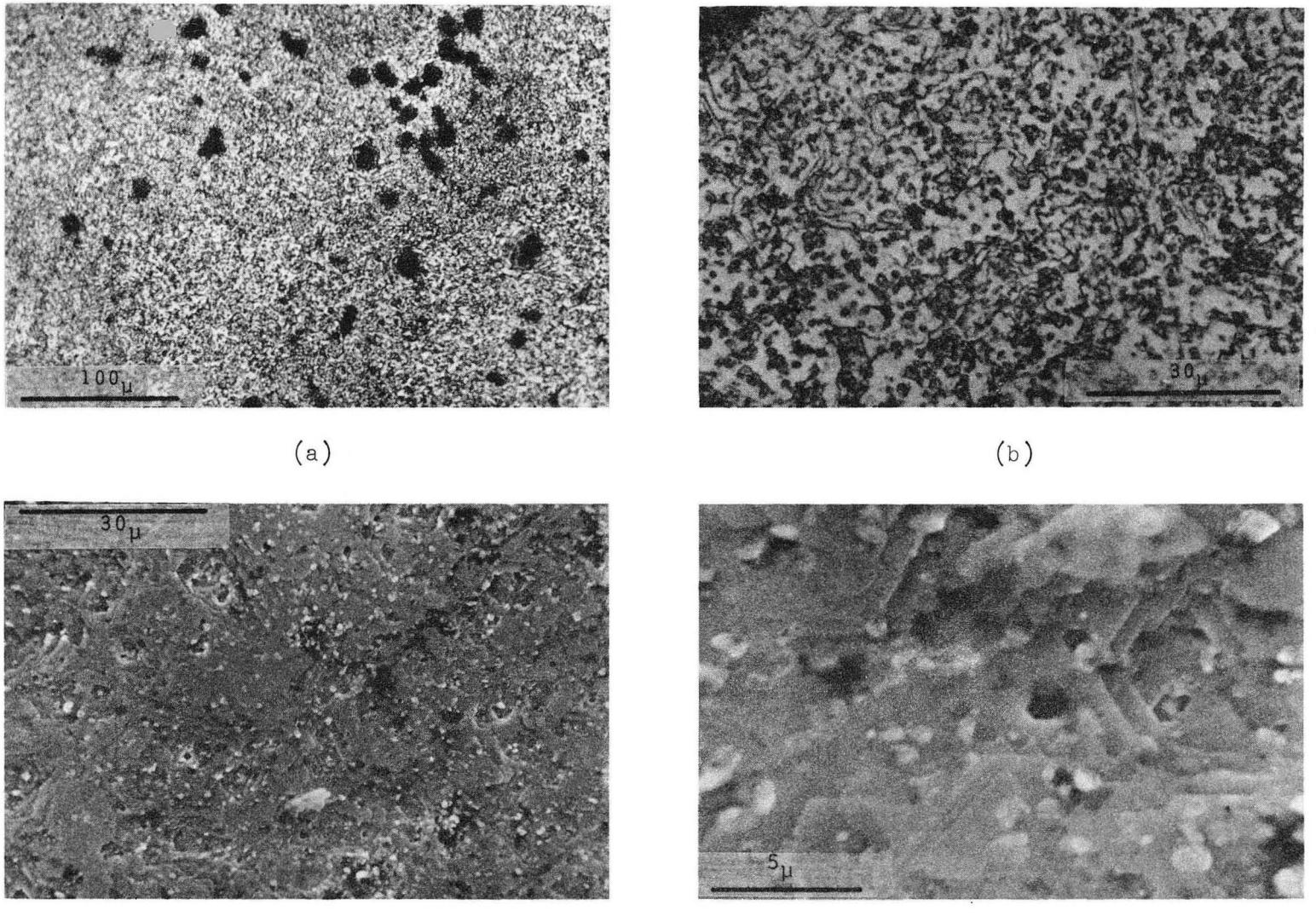

Fig. 20 (0001) surface of grown zinc which sublimed with crystal edges exposed. Comparison with Fig. 19 shows different behavior of different crystal batches.

In this investigation hillock formation for the high purity zinc is associated with zinc oxide segregation.

Evaporation pits originating at screw dislocations in the manner analyzed by Cabrera and Levine[17] are not expected to be observable by the microscopic techniques used in this investigation. The development of Cabrara and Levine has shown that the spiral ledge to ledge spacing attains a limiting value of $d = 19\rho_c$ within a very short distance from the center of the dislocation. ρ_c is the critical radius of two dimensional nucleation of adsorbed atoms, and is given by

$$\rho_c = \frac{\gamma\Omega}{kT\ln C/C_o}$$

where γ is the surface free energy, Ω is the atomic volume, and C_o and C are the vapor pressures at equilibrium and experimental conditions respectively.

For zinc, γ was estimated to be 955 ergs/cm^2 from the expression

$$\gamma = \frac{n\Delta H_{sub}}{4N_A}$$ [54]

where n is the number of atoms/cm^2, ΔH the heat of sublimation, and N_A is Avogadros number. This leads to an estimated ledge to ledge spacing of .02μ. The slope of a pit, given by the ratio of an atomic diameter of 2.35Å to 200Å, is about 41' from the surface plane. Such a low angle is not detectable under usual microscopic techniques. The fact that no pits were seen on the high purity zinc does not prove that

spiral ledges were unimportant in the sublimation mechanism. However, the separation of ridges and hillocks in of the order of 50 to 100μ and it seems probable that these surface features define the distances over which zinc oxide particles were pulled by advancing zinc ledges. If the high measured value of α for the high purity zinc were accounted for by the dislocation density required by the Hirth and Pound theory, the ridges should be much more closely spaced. It seems certain that a much lower concentration of ledge sources than predicted by Hirth and Pound theory is required to maintain the equilibrium flux from a high purity (0001) zinc surface.

The causes of the thermal pits and lowered evaporation coefficient observed on the less pure grown zinc is not definitely known. Large thermal pits have been observed previously[20,55-58] and they have been described as arising from clusters of dislocations.[19] However, this investigation shows that these pits can develop from a single micropit (Fig. 14). Whether this pit emanates from a dislocation or not cannot be said with any certainty.

The only apparent difference between the commercial zinc and the grown zinc was that the commercially purchased zinc was of exceptionally high purity. Etch pit studies showed that both types of zinc had about the same dislocation densities. The fact that ledges and pits formed on the grown zinc but not on the high purity zinc might be explained by the difference in impurity level. Young and Gwathney[59] have encountered similar differences in their work on copper spheres.

They evaporated copper spheres in vacuum and observed the morphological

development at the (111), (101), and (1$\bar{1}$0) poles. A copper sphere that had no detectable impurities developed very differently than a sphere that was only 99.8% copper.

For many metals, chemical etching does not reveal etch pits unless the dislocations are decorated with a certain concentration of impurity atoms.[60] It is felt by some that poisoning or impurity effects are needed for the pileup of ledges and the formation of pits upon evaporation.[61,20] Perhaps thermal pitting and the lowered evaporation coefficient for the grown zinc both arise because impurities reduce the rate of advance of microledges.

Edge exposed experiments on one batch of crystals resulted in surfaces which were extremely flat with no signs of pitting or ledges. The surface from another batch of crystals showed some pitting and ledge structure (compare Figs. 19 and 20). The difference between samples may have been caused by slightly different impurity levels.

Presumably, the bulk impurities in the grown sample were effective in altering the rate of free surface sublimation as well as affecting the surface morphology. On the other hand, impurities and artifacts associated with only the surface (e.g. ZnO formation on the surface) had no apparent effect on the rate of sublimation or morphological development.

It appears that surface edges were such ready sources for ledges that the surface recession produced by sublimation of edge generated ledges proceeds faster than pits can penetrate into the surface. Since this observation suggests that the sublimation coefficient for the grown crystal (0001) face with the crystal edges exposed might increase above

the 0.7 measured with the surfaces collimated, attempts were made to measure the sublimation flux from surfaces with the edges exposed. The evaporation coefficient obtained with these attempts was 1.1. However, the experimental error is difficult to estimate because of the unknown contribution to the torque of sublimation from the sides of the crystal and of the area changes as the (0001) surface erodes away from the edge.

The dislocation densities of samples used in this investigation varied from 10^4 to 10^5 line/cm^2. This variation caused no noticeable corresponding variation in the free surface sublimation flux, although it cannot be said whether the scatter of the free surface data (see Fig. 6) is related to different dislocation densities or not. The effect of dislocation densities on the rate of sublimation was not systematically studied because due to the slip plane being the (0001) plane, one cannot methodically alter the number of dislocations intersecting the (0001) surface and at the same time keep all the variables constant (e.g. number of dislocations lying in (0001) plane).

The results presented here give strong indications that the Hirth and Pound prediction of α equal to 1/3 for low index surfaces with less than 10^6 dislocations/cm^2 in incorrect. Samples with dislocation densities as low as 9×10^3 lines/cm^2 were characterized by an evaporation coefficient of unity. Such a low density of dislocations intersecting the basal plane of zinc is not unexpected because of the one dominant slip system of zinc. Any dislocations introduced by handling the crystal lie in the (0001) plane and do not intersect it. The densities observed

in this investigation were comparable with previously reported dislocation densities in the (0001) plane of zinc, Ruff[35] observed densities on the order of 3×10^4 pits/cm^2 using the same etchant as in this investigation, and Sharp[34] found densities of 4×10^5 pits/cm^2 using a different etchant.

V. NON-STEADY STATE FREE SURFACE SUBLIMATION

A. Development of Surface Morphology

Initial induction periods which must be passed before the sublimation flux reaches the steady state values have been observed in a number of previous investigations.[28,62] Apparently, however, the fluxes measured in previous studies have always been within a factor of 2 or 3 of the steady state pressure and no detailed study of this non-steady state sublimation period has been reported. The sensitivity of the torsion-Langmuir method has made it possible to measure the flux of zinc continuously from an initial value about 2 orders of magnitude below the steady state value.

A typical plot of pressure versus time at constant temperature for free surface sublimation from the basal plane of crystals grown in this laboratory is shown by curve a on Fig. 21. The corresponding heating curve is shown by curve t of Fig. 21. There was a slow rise to the steady state pressure region.

The structure of the surface during the period of pressure increase is depicted on Figs. 22a - 22h. Figure 22a shows the distribution of pits as they initially formed on the surface. Pits preferentially formed at cleavage steps, slip lines, and scratches. In many instances pits tended to form in straight lines and when pit density was high, coalescence of these pits resulted in canal-like features (Fig. 39). But many pits also formed with random distribution in areas apparently free of surface defects. Pit distributions were very non-uniform over any particular sample surface.

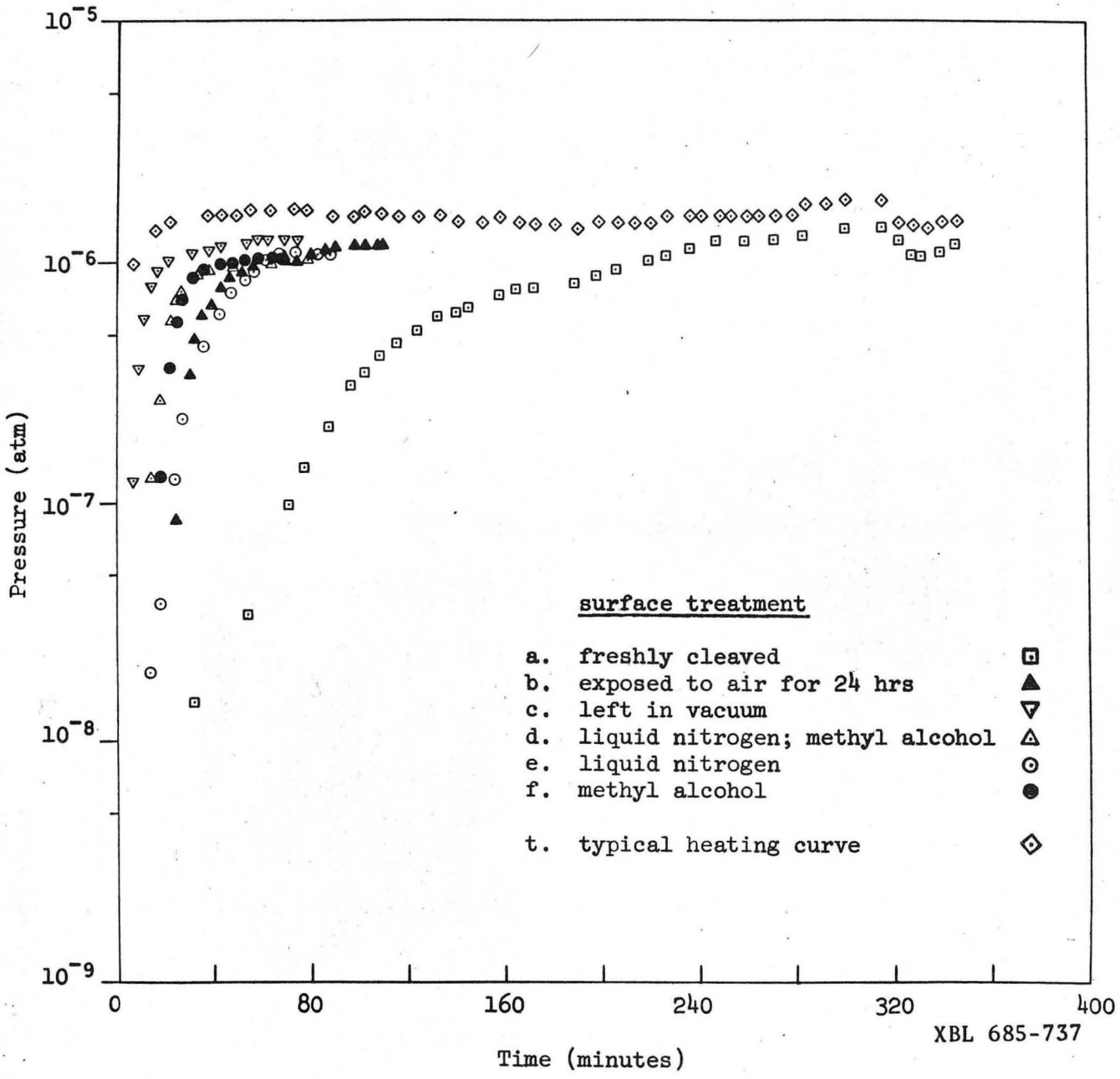

Fig. 21. Pressure dependence on time of (0001) surface of grown zinc at constant temperature and varying surface treatments.

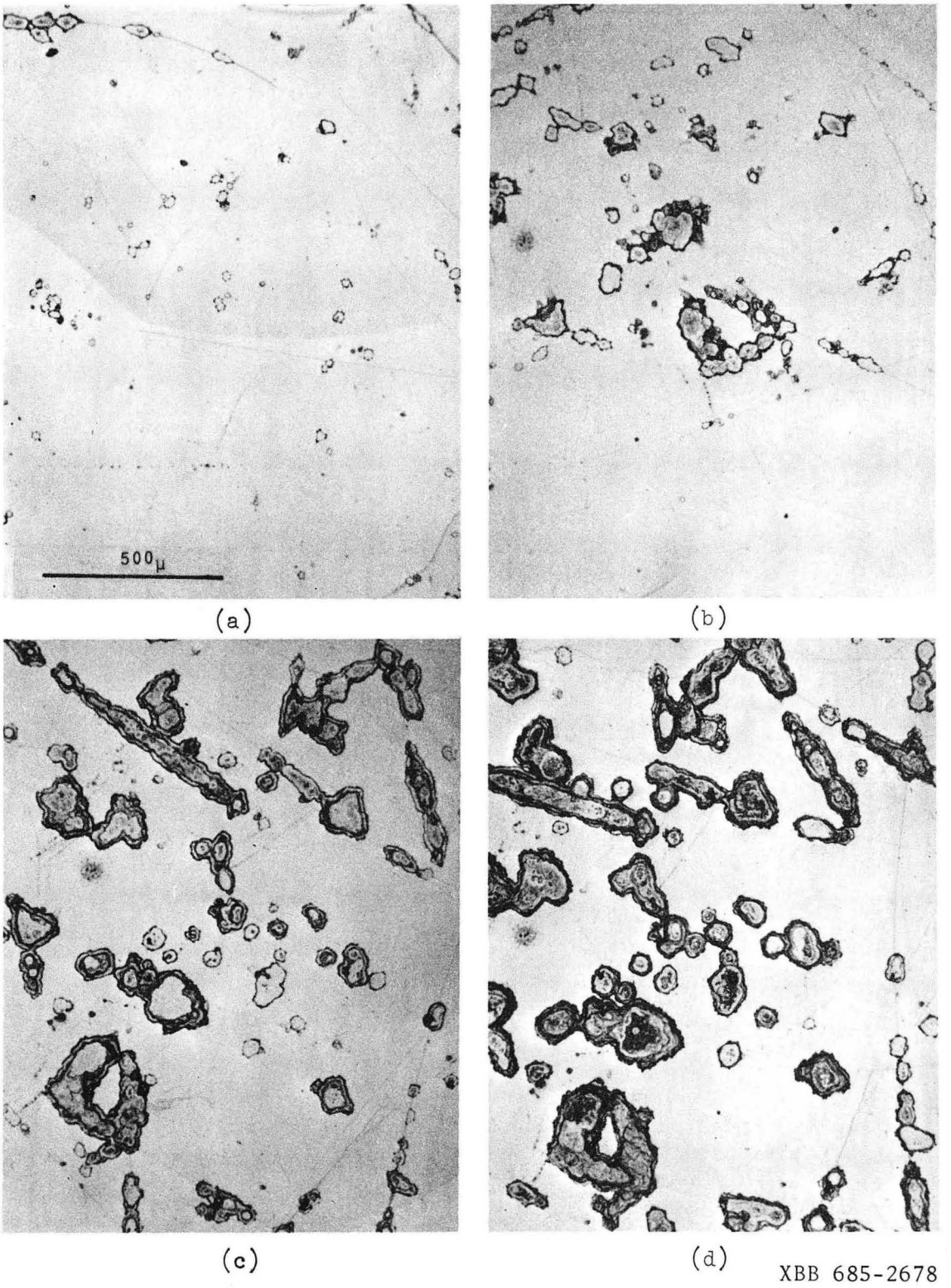

Fig. 22 Development of (0001) surface of grown zinc in non-steady state region as a function of time.

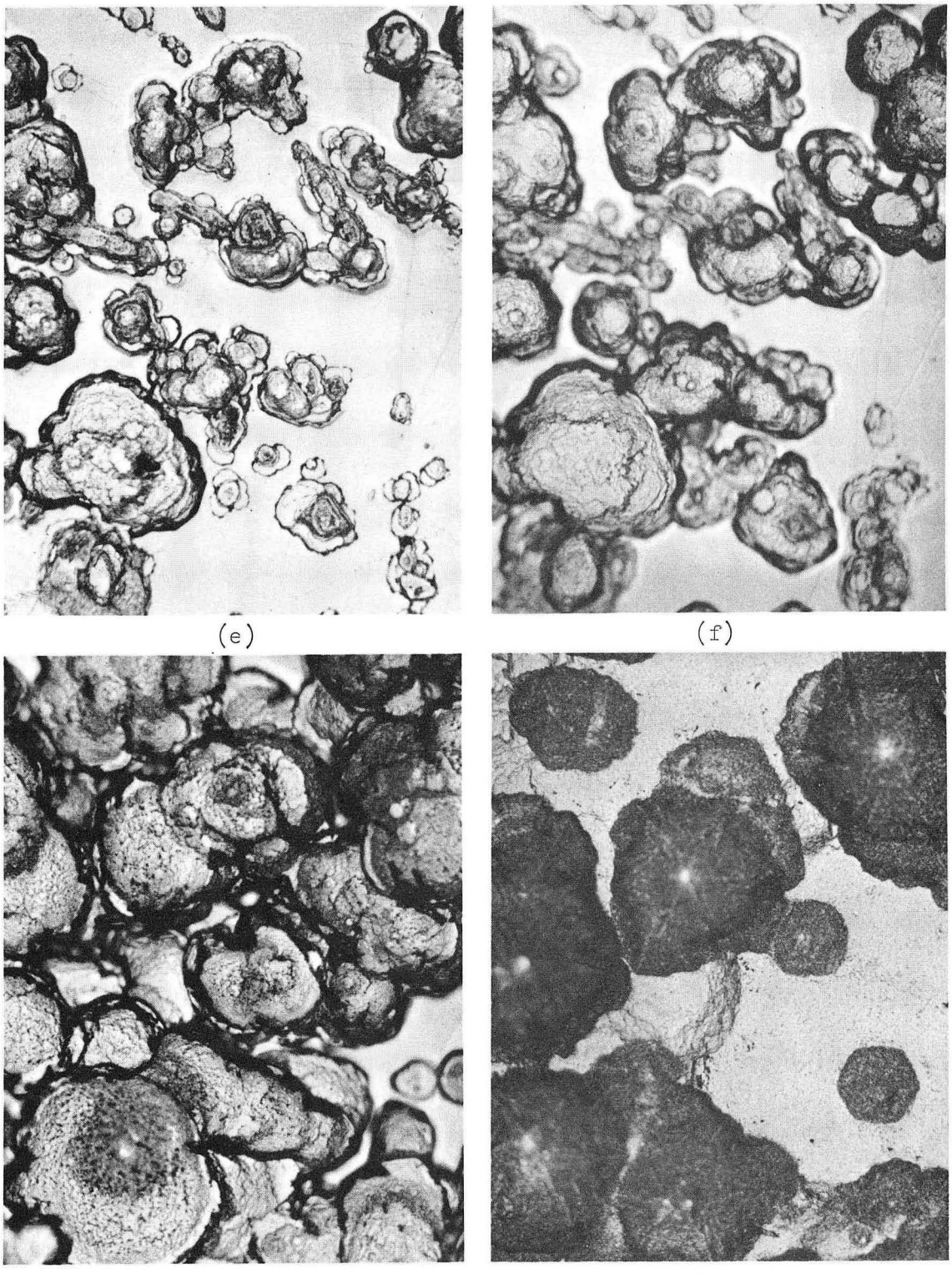

(e) (f)

(g) (h)

XBB 685-2683

Fig. 22. (cont.)

All of the initial pits were hexagonal in cross section. Some of the pits were relatively smooth on the bottom (Fig. 23-a) and some of the pits developed some relief (Fig. 23-b).

The concentration of pits observed for various grown zinc surfaces ranged from 1.0×10^3 to 3.0×10^4 pits/cm^2, and the number of pits did not increase with time of sublimation. Instead, many of the pits widened while some of the pits remained inactive. The expanding pits were predominantly of the types depicted in Figs. 24 and 25. Some were distinctly terraced so that (0001) surface planes remained dominant (Fig. 24). The sides of the pit walls near the top became almost vertical as though sublimation of the original cleaved surface remained much slower than sublimation from inside the pits. The bottom surfaces were flat but showed some roughening during later stages of development.

The terraced structure did not result from contamination when the surfaces were exposed to air for examination between sublimation runs; some samples which were heated directly to this stage of development showed similar terraces.

Some pits were associated with one source of ledges and other had several. Figure 25 shows a closely spaced pair of hexagonal pits which acted basically as a single source.

Pits which were inactive and did not spread were like that represented in Fig. 23-a. They were not stepped or terraced over their broad flat bottom. But, the edges of the pits were very steeply ledged, like those of active pits.

With time, the active pits continued to broaden and deepen while the

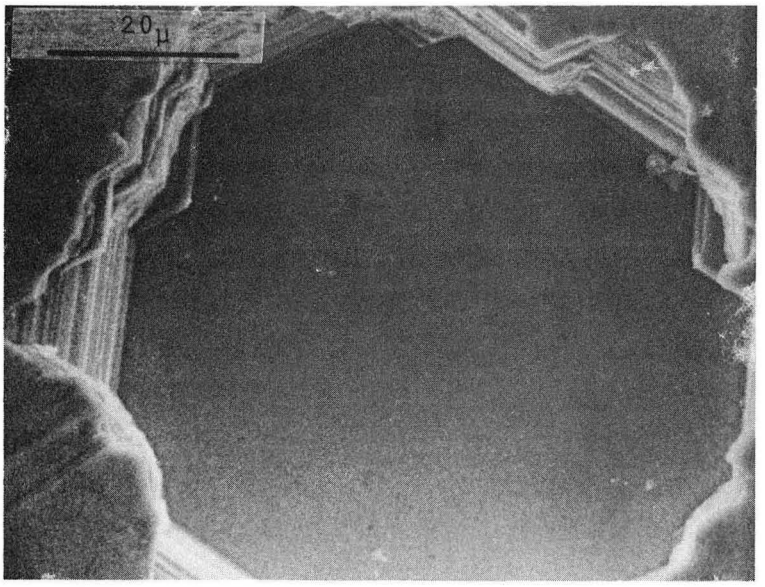

(a)

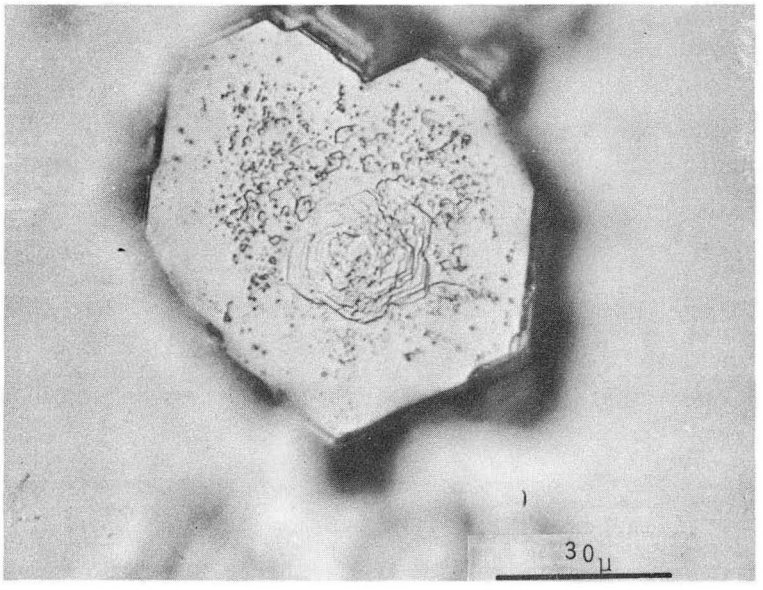

(b) XBB 687-4172

Fig. 23 Two types of initial thermal pits formed on a cleaved (0001) surface of grown zinc.

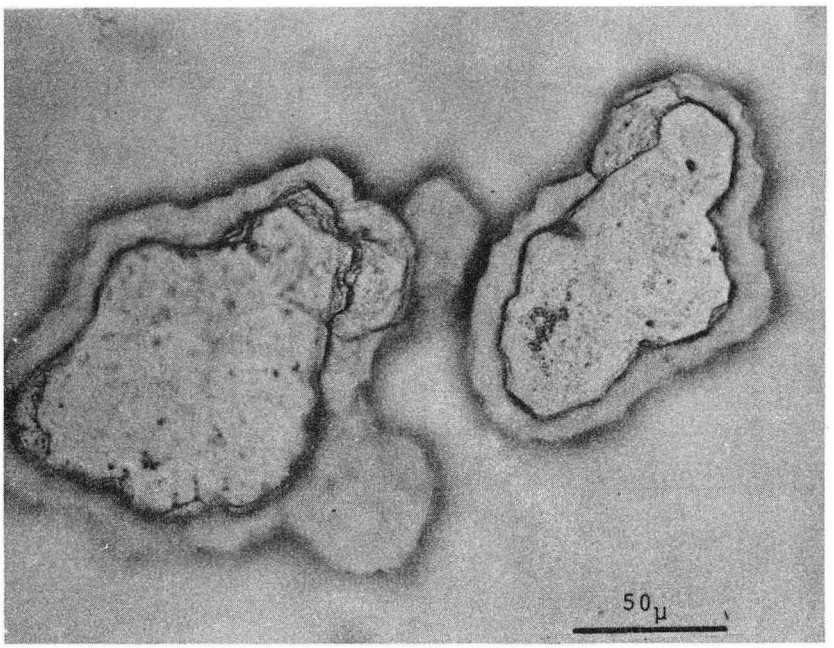

(a)

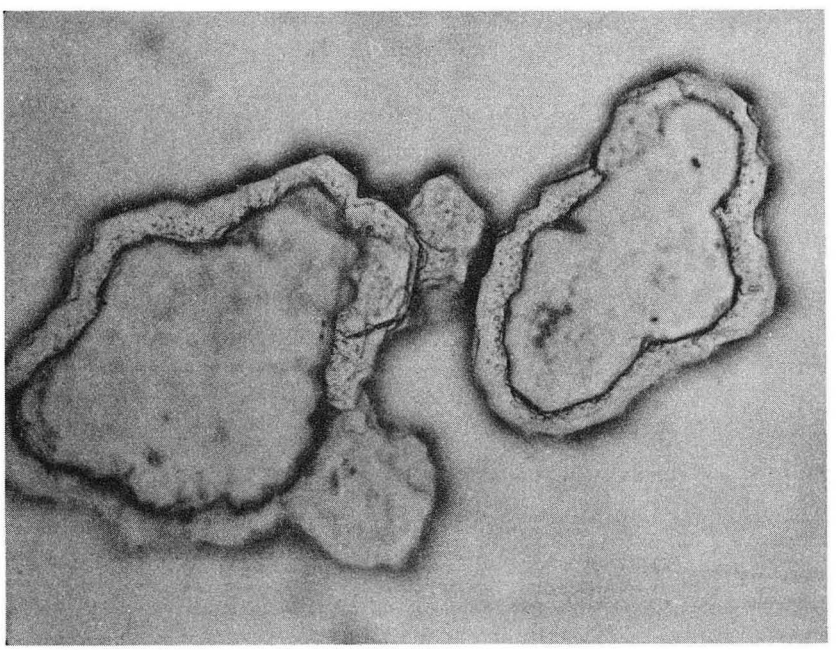

(b) XBB 687-4173

Fig. 24 Optical micrographs of actively spreading pits of terraced nature.
(a) focused on the bottom
(b) focused on terrace

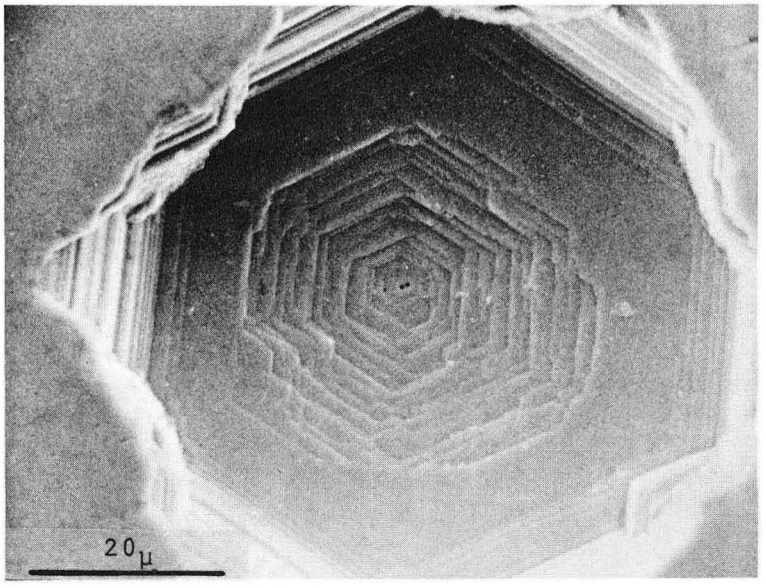

XBB 687-4174

Fig. 25 Electron micrograph of an active spreading pit associated with a single source of ledges.

relatively inactive pits usually remained dormant until they disappeared under the advance of active pits. However, as seen in Fig. 22, some pits which were inactive in the early stages became very active and some active pits nearly ceased to spread after a certain time.

Eventually there were two distinct types of pits (Fig. 26). Figure 26-a shows an active pit. It is seen that many ledges emanated from this pit and there was much relief associated with it. Figure 26-b shows the relatively smooth and structureless surface of a nonactive pit.

The general overall appearance of a (0001) surface after sublimation had reached about 90% of the steady state level is shown on Fig. 22-g. It is seen that the surface appears quite rough. All relatively inactive pits had now been annihilated. Closer examination of the large pits that remained at this point showed that most of them contained a number of smaller pits (Fig. 27).

At the time that steady state pressures were reached, continued broadening of the active pits had yielded a relatively flat sample surface. The concentration of large pits at this stage ranged from 6 pits/mm^2 down to none at all. The further development of surface morphology in the steady state region has been discussed on pages 29-48 and is depicted on Fig. 10.

The non-steady state behavior of the (0001) surface of the high purity zinc was also studied, although not as extensively as for the grown crystal. The pressure versus time behavior as shown in Fig. 28 is very similar to those of Fig. 21. The morphological development of the surface as a function of time is shown on Fig. 29.

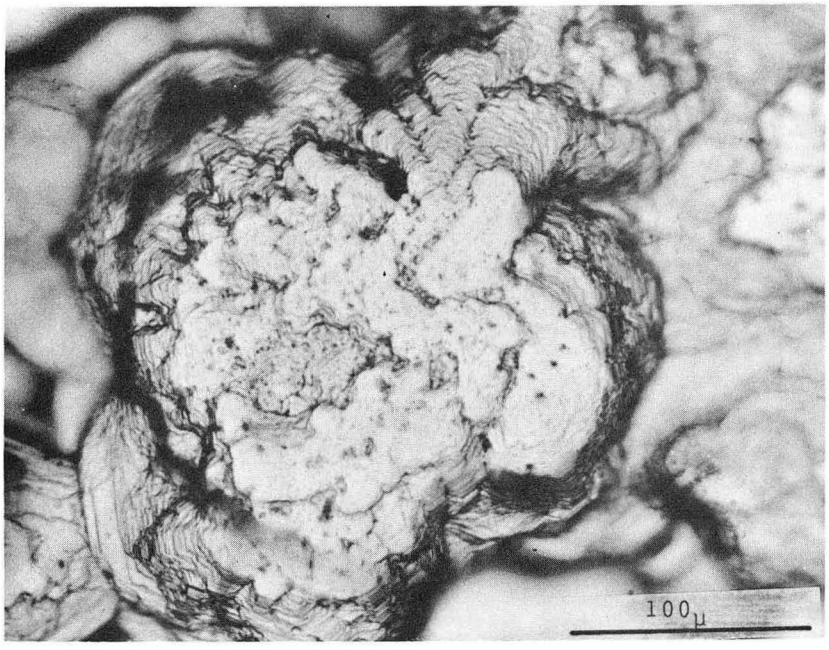

(a)

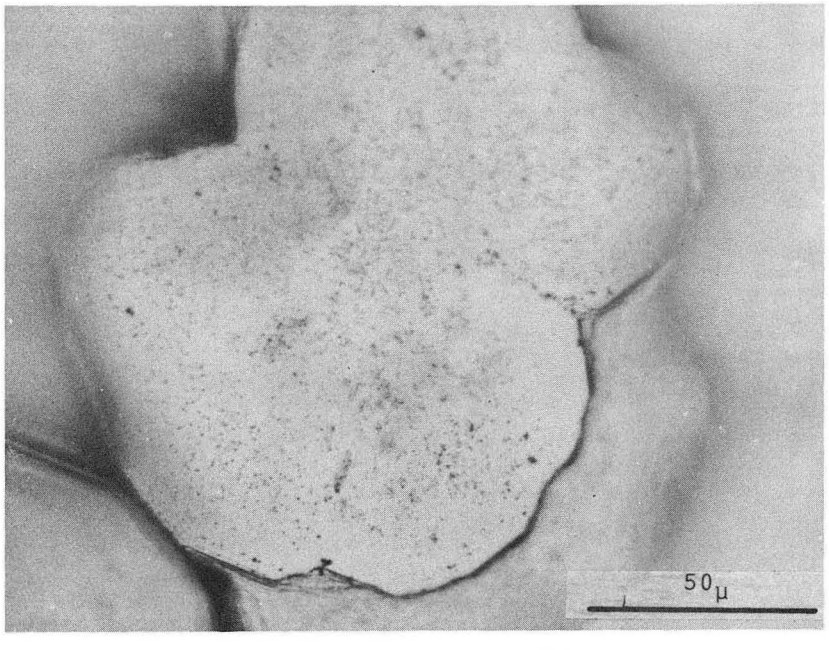

(b) XBB 687-4175

Fig. 26 Optical micrographs of two types of pits during the non-steady state sublimation. (a) is an actively spreading pit and (b) is inactive.

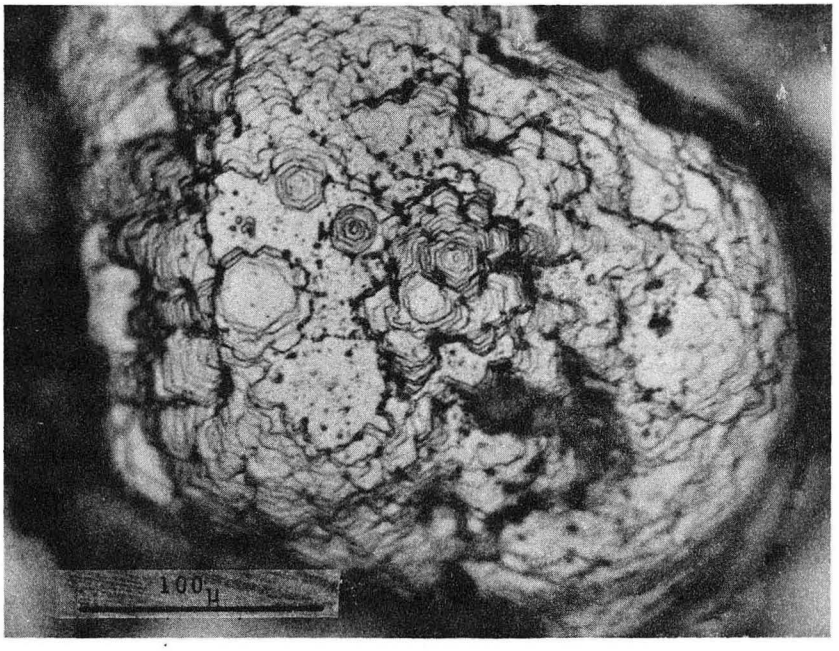

XBB 687-4176

Fig. 27 Typical pitted area when 90% of the cleaved surface had been annihilated.

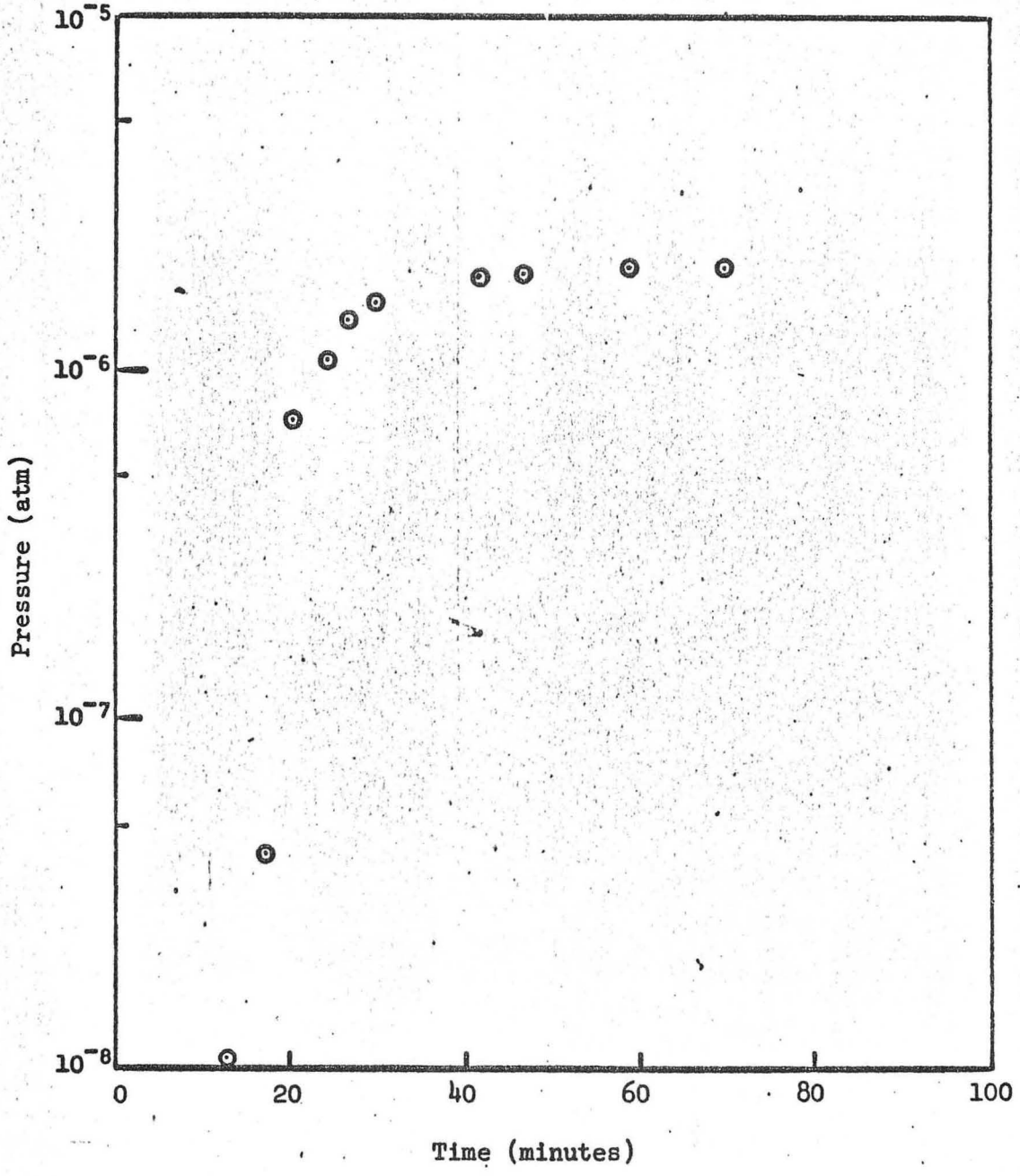

Fig. 28. Pressure dependence on time of cleaved (0001) surface of high purity zinc.

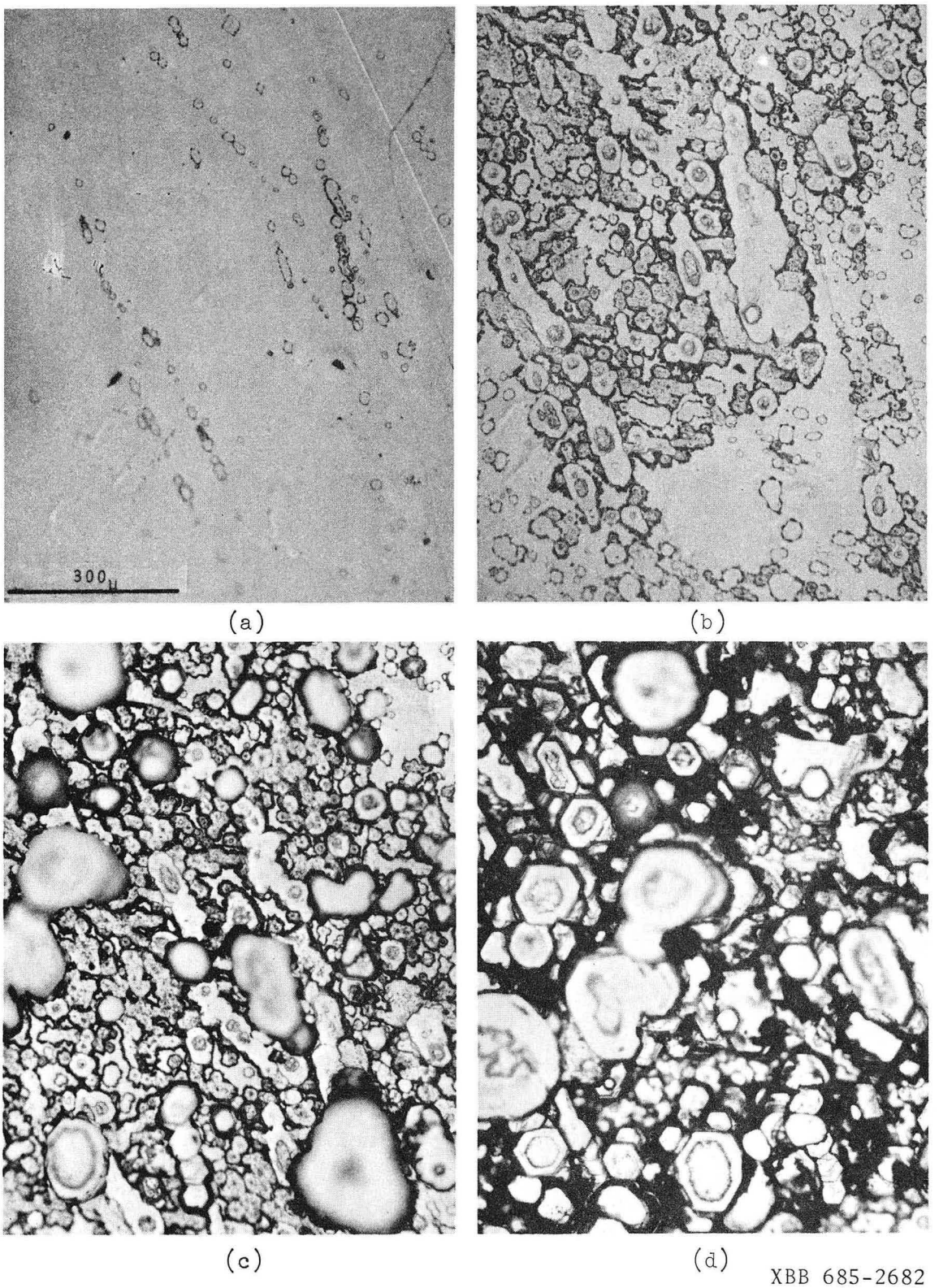

Fig. 29 Development of (0001) surface of high purity zinc in non-steady state region as a function of time.

For the high purity zinc, sublimation also proceeded by formation and spreading of pits, and steady state pressures were attained when all of the original cleaved surface was eliminated by the spreading pits. As observed with the grown crystals, some pits were extremely active and some were inactive in the sublimation process.

There were however several distinct differences. For the high purity zinc the concentration of pits averaged higher than for the grown zinc. The initial pit densities for the high purity zinc ranged from 9×10^3 to 4×10^4 pits/cm^2. These values are all near the maximum density for grown crystal surfaces. All pits in high purity zinc had distinct hexagonal features, while the geometry of the features in pits in the grown zinc were not as well defined (compare for example Fig. 26-a with Fig. 30).

Figure 30 shows the regular ledge formation at the bottom of a spreading pit. Note that the great amount of irregular relief and clover-shaped ledges which are seen in Fig. 26-a is not found in Fig. 30, although the two pits are depicted at about the same stage of surface development. Most of the large pits roughened on the bottom (Fig. 31) and the largest pits developed smaller hexagonal pits on their bottoms (Fig. 32). Absent were the swirling type of pits observed so frequently in the grown crystals such as those observed in Fig. 27.

The non-steady state region for grown crystals with the edges exposed was also examined. Upon heating at constant temperature, the pressure increased with time in a manner similar to the runs shown on Fig. 21 (Fig. 33). Pits developed and spread on the surface as before.

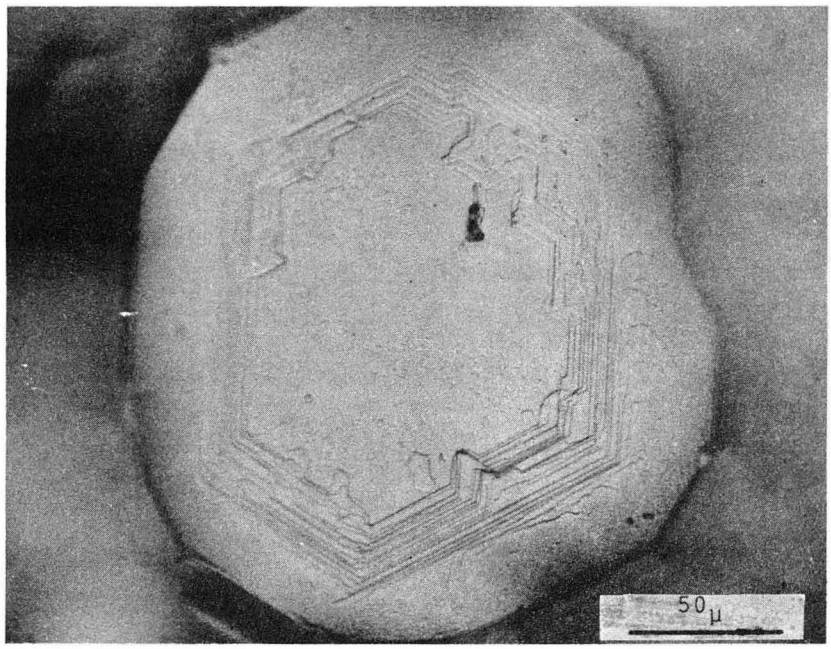

Fig. 30 Typical pit formed on (0001) surface of high purity zinc during non-steady state sublimation.

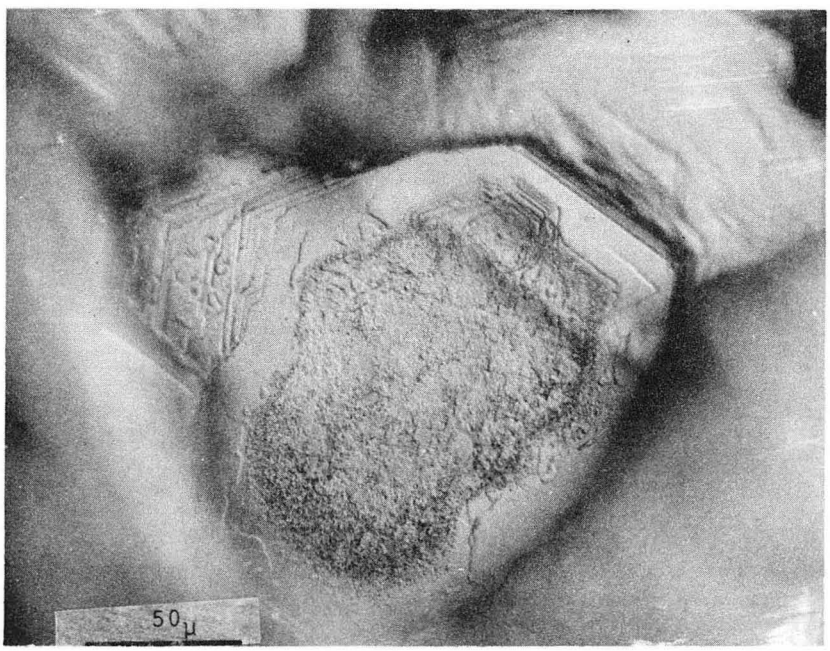

XBB 687-4177

Fig. 31 Pits of the type shown on Fig. 30 roughened with time.

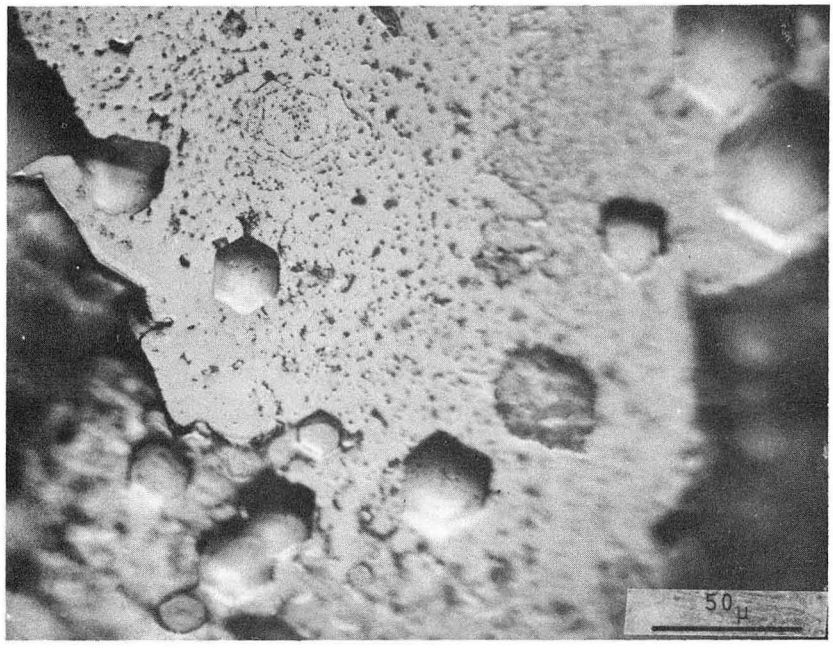

XBB 687-4178

Fig. 32 Pit development within a large pit on the (0001) surface of high purity zinc. Compare with Fig. 27 for comparable stage of development on grown zinc.

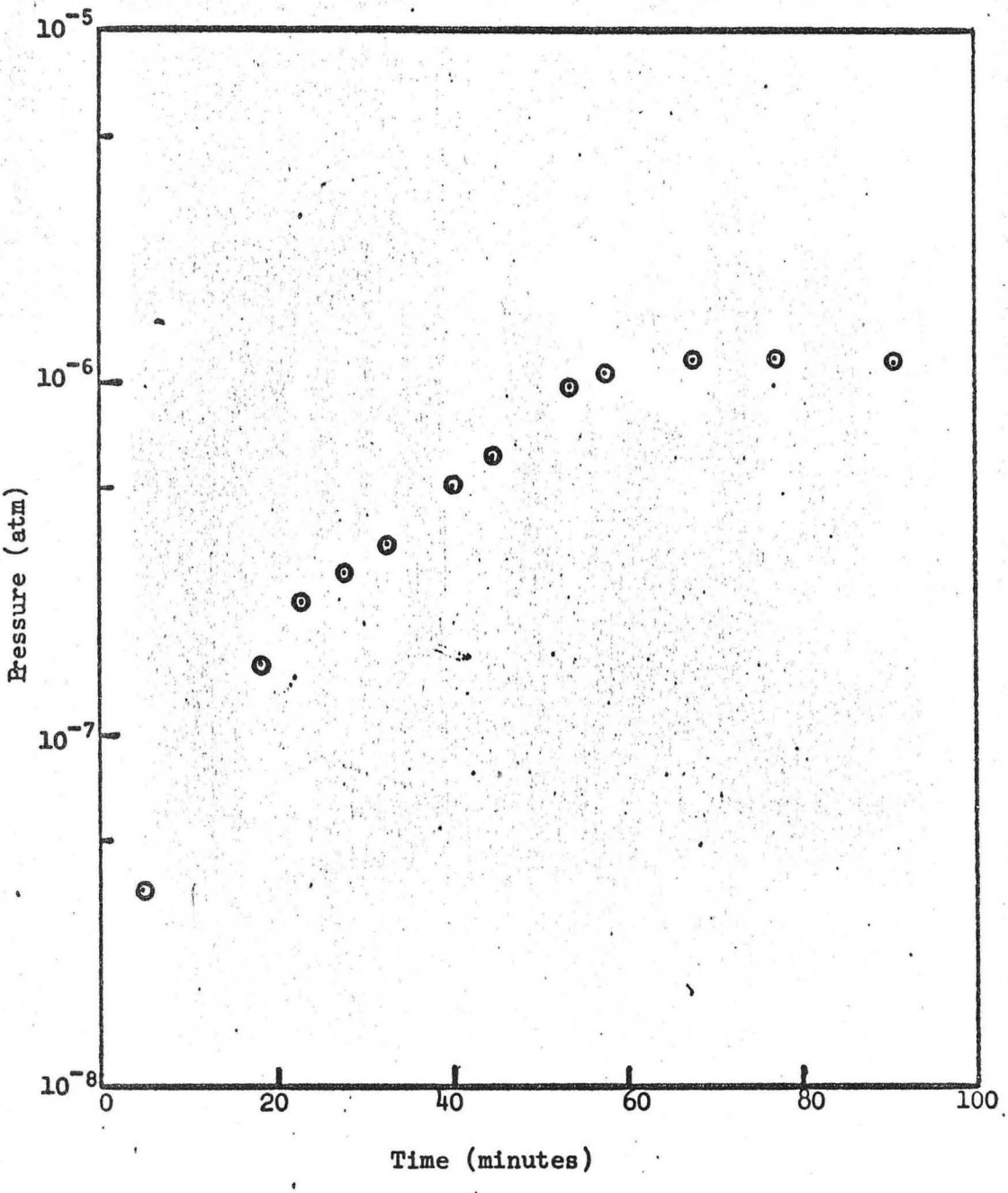

Fig. 33. Pressure dependence on time of cleaved (0001) surface of grown zinc with edges exposed.

the sample observed had about 1 x 10^3 pits/cm^2, and the pits closely resembled those pictured in Fig. 22.

Sublimation was also initiated at the exposed edges at areas that looked like sections of flat hexagonal pits (Fig. 34). With time, the active areas near the edges developed relief similar to that of pits near the center of the (0001) surface.

Once the entire original cleaved surface had been eliminated, the surface leveled and sublimation in the steady state region failed to produce more pits.

B. Correlation between Thermal Pits and Dislocations

Attempts were made to see if the thermal pits formed at points where dislocations intersected the surface. Several matching faces of cleaved grown crystals were thermally and chemically etched, and the resulting pit distributions were compared. Figure 35 shows an example of two matching surfaces. Cleavage cracks and scratches were effective points of nucleation of the active type of pit. Some matching halves showed bands of pits in the same areas which were running the same direction. However, the thermal pit density was always lower than that of the etch pits. At points removed from gross imperfections such as cracks and scratches, the pitting in the separate surfaces of some pairs showed absolutely no relationship with each other. The chemical etch pit density might be on the order of 10^5 pits/cm^2 while the thermal pit density was only about 10^4 pits/cm^2.

In one series of experiments, surfaces were chemically etched, the etch pit distribution was observed, and then the surface was thermally

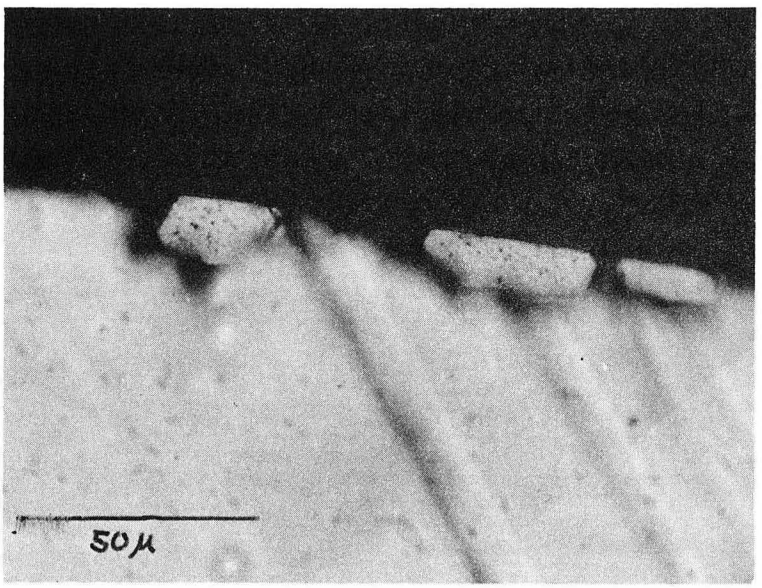

XBB 687-4179

Fig. 34 Evaporation pits initiated at the crystal edge during the non-steady state sublimation.

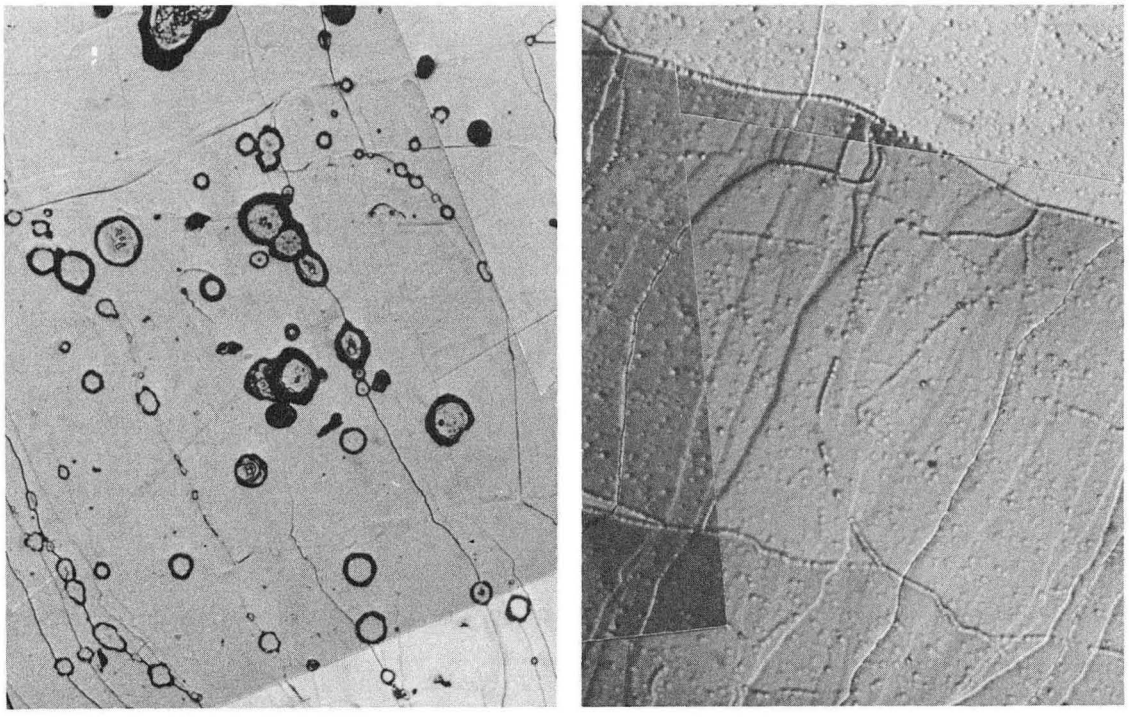

XBB 685-2679

Fig. 35 Thermal and chemical etch patterns on two matching halves of a cleaved grown zinc crystal.

etched so that the concentration and distribution of thermal etch pits relative to chemical pits could be measured.

A typical area of a surface after this series of treatments is shown on Fig. 36. It is seen that thermal pitting took place at both etched and unetched areas, and that most points of dislocation intersections were inactive in producing thermal pits. The possibility exists of course, that thermal etching at dislocation sites would be inhibited by previous chemical etching at these sites. But the concentration of thermal etch pits formed was comparable with the concentration on surfaces which were not subjected to previous chemical etching.

One surface was thermally etched and then chemically etched. Most thermal pits did not develop chemical etch pits, and 20 times as many chemical etch pits as thermal etch pits were produced.

To further test whether thermal pits correspond to crystal defects, a grown crystal was cleaved and thermal pit patterns on the two matching halves of the crystal subjected to extensive thermal etching were compared. (Fig. 37). Pitting clearly tended to form preferentially for both halves along matched linear bands. But there was not complete matching for all pits.

Therefore, it appears that cracks, scratches and dislocation intersections are sources for thermal pitting, and only a small fraction of dislocation intersections became the origins of thermal pits. This result is consistant with observations for other systems.[63,59]

The thermal etch technique has been studied as a method for determining dislocation densities. Heating in vacuo does not seem sufficient

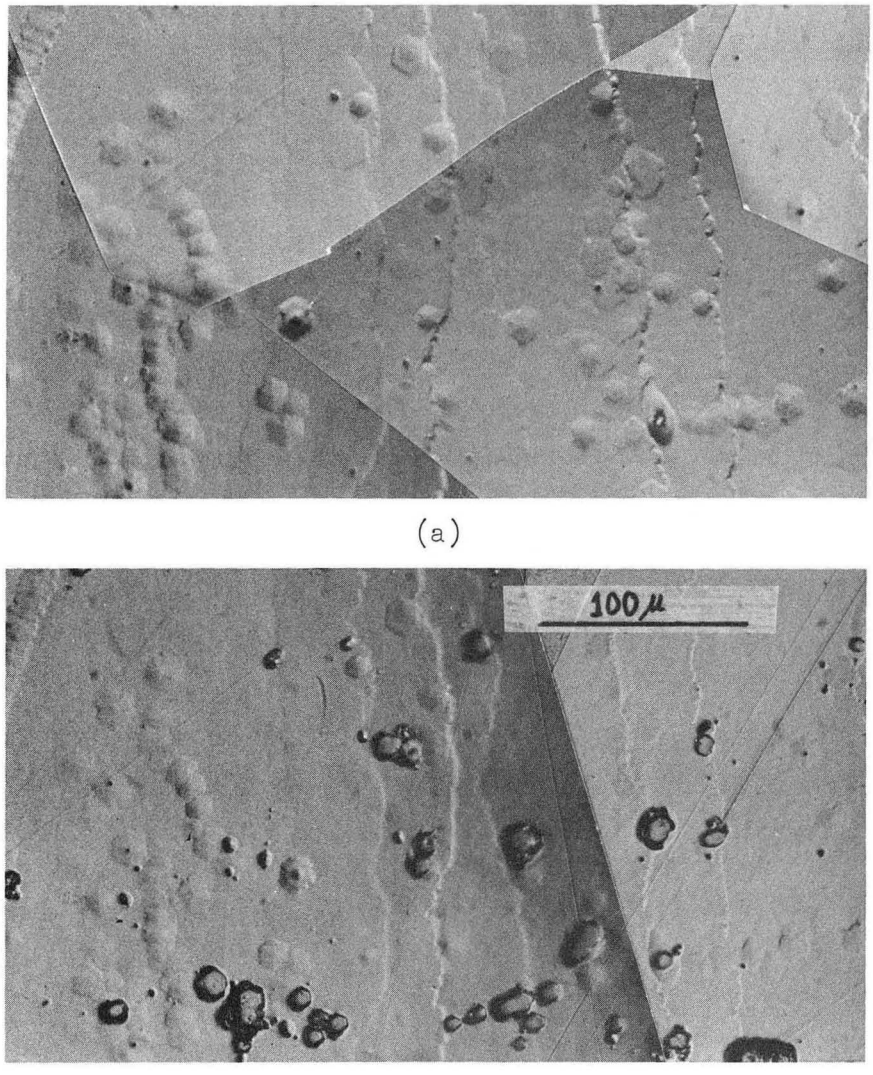

(a)

(b)

XBB 685-2680

Fig. 36 (a) Chemically etched (0001) surface of grown zinc. (b) Same surface after subsequent thermal etch.

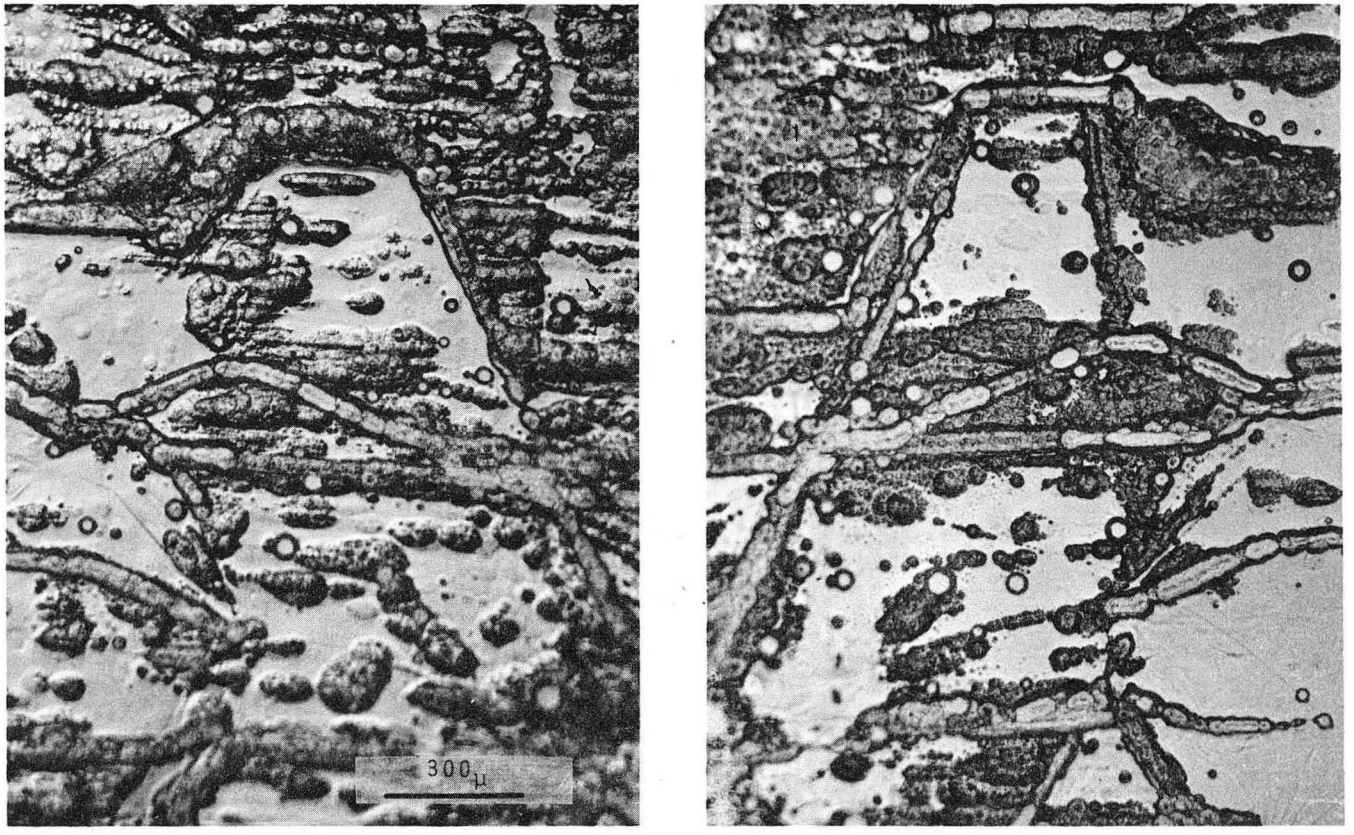

XBB 687-4180

Fig. 37 Thermal etch patterns on two matching halves of a cleaved grown crystal of zinc.

to produce a one to one correspondence between thermal pits and dislocations. It is believed that a chemical agent must be present during heating. Close correlation between thermal pits and dislocation intersections has been established for silver heated in oxygen,[64] chromium heated in hydrogen,[65] and copper with oxide impurities.[66]

It was found that surfaces prepared in identical ways from the same crystal rod showed wide variations in their rates of approach to the steady state pressure. Figure 38 shows the rate of pressure increase up to a pressure about one order of magnitude less than the steady state pressure for 4 different samples of the grown zinc. The appearance of the various surfaces when the measured pressures had reached this level is shown on Fig. 39, where Figs. 39-a, 39-b, 39-c, and 39-d correspond to curves, a, b, c, and d of Fig. 38 respectively. It is seen that the faster the rate of increase in pressure, the greater the density of thermal pits. Densities ranged from 1.3×10^3 pits/cm^2 for sample d to 3.8×10^4 pits/cm^2 for sample a. The chemical etch studies revealed that dislocation counts varied from 3.3×10^4 lines/cm^2 to 5.3×10^5 lines/cm^2 for the most imperfect surfaces. This suggests that perhaps one out of every ten dislocations are active in forming a thermal pit, and that the variation from sample to sample as shown on Fig. 39 reflects the difference in dislocation densities. However, it is hard to believe that dislocation densities would vary over an order of magnitude in different positions of the same crystal rod.

C. Effects of Surface Contaminants

A series of experiments were performed in an attempt to determine why the initial sublimation rates are far below the steady state rates

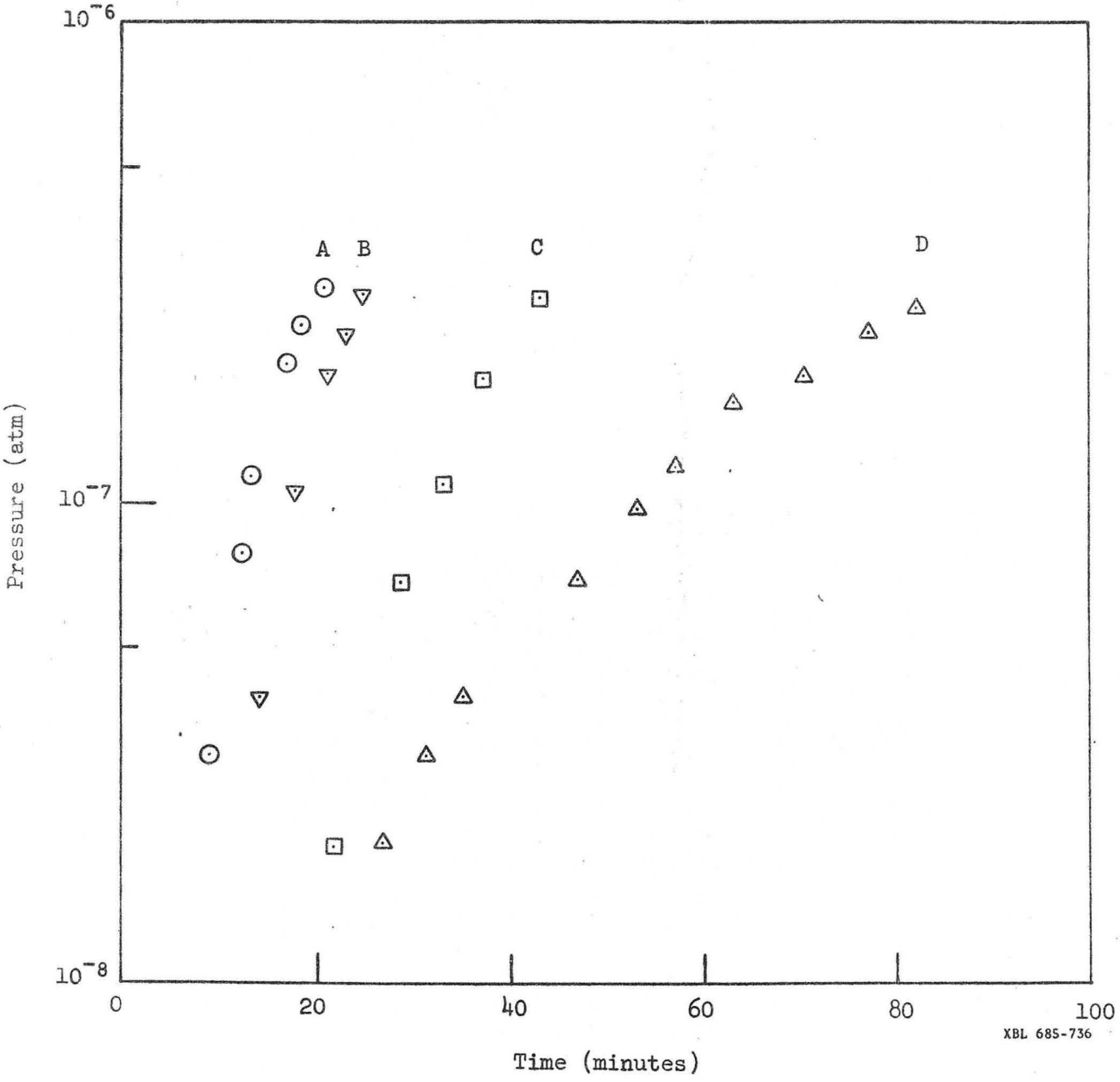

Fig. 38. Rate of pressure increase with time in the non-steady state region for various grown zinc samples.

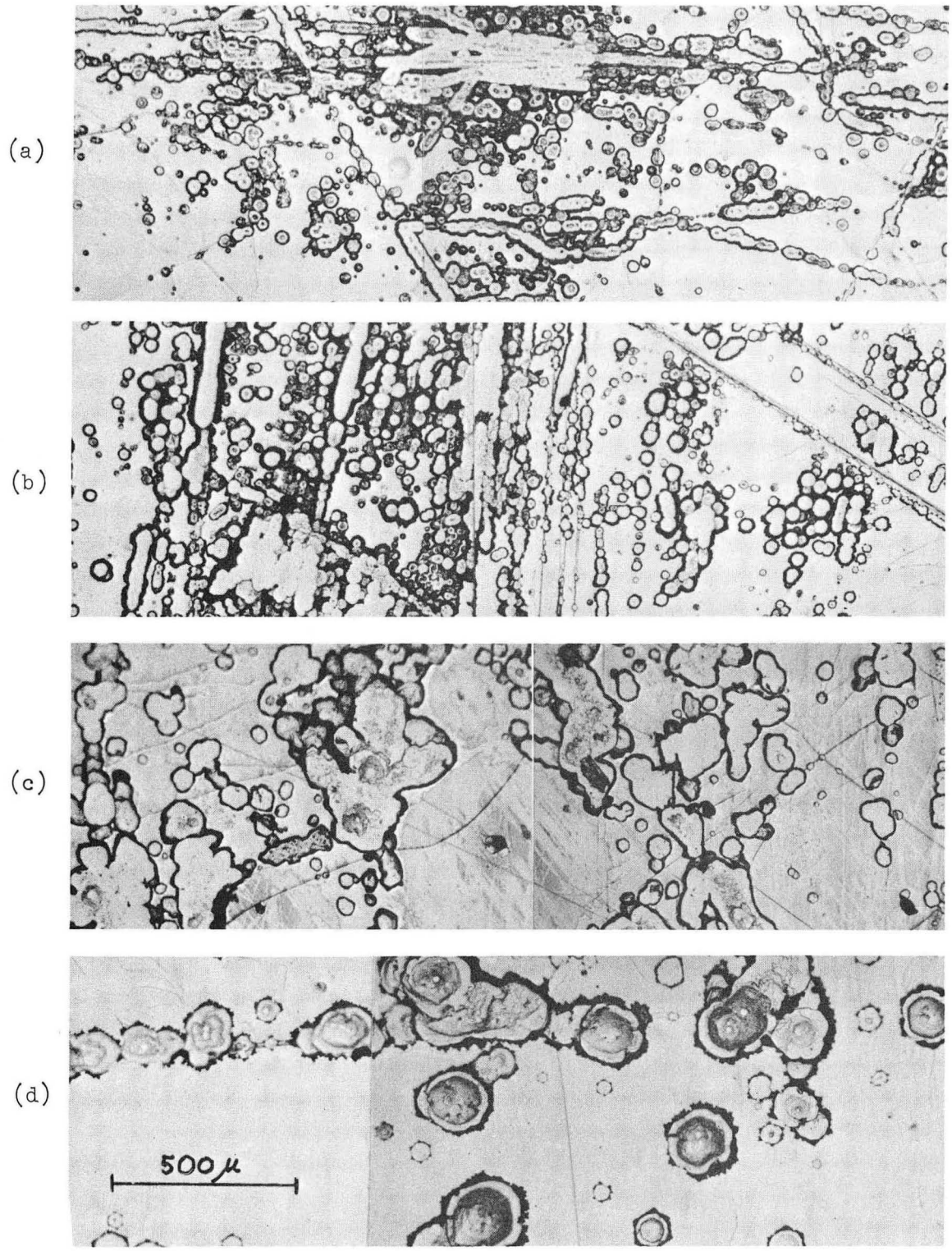

XBB 685-2684

Fig. 39 Appearance of the (0001) surface of various grown zinc samples at approximately the same non-steady state pressure. Correlate these surfaces with the curves of Fig. 38.

and what changes in sample conditions are responsible for the widely varying rates of approach to the steady state. It seemed likely that impurities which became adsorbed in the crystal surfaces during the preparation of samples might markedly influence the early stages of sublimation.

Figure 21 summarizes results of experiments designed to see what influence crystal preparation technqiues exerted on the sublimation behavior. Curve a shows the behavior of a typical cleaved surface. The heating curve corresponding to this run is also given as curve t on Fig. 21. From comparison with the curves of Fig. 38, the thermal pit density was estimated to be on the order of 10^3 pits/cm^2 for this particular sample.

Steady state pressures were reached after 245 minutes. The pressure measurements were continued for an additional 100 minutes into the steady state region and there were no further changes in pressure except for minor fluctuations which directly reflected small fluctuations of temperature with time. The surfaces at the end of this run looked like that depicted on Fig. 22h.

The sample was removed from the vacuum chamber, exposed to air at room temperature for 24 hours, and then was reheated with a heating schedule identical to that used in run a. The resulting pressure versus time curve is curve b on Fig. 21. Steady state pressures were reached within 90 minutes. The sample of run b was left under vacuo until it had cooled to about 345°K and was then heated as before. The result is shown as curve c, Fig. 21, where it is seen that the time required to

reach the steady state pressure was reduced to 30 minutes.

The sample from c was then soaked in liquid nitrogen and transferred to a methyl alcohol bath. On heating, the sample showed a rather fast rise to the steady state as indicated by curve d of Fig. 21. The separate effects on the induction period of methyl alcohol and liquid nitrogen are seen on curves e and f of Fig. 21. The methyl alcohol effect was examined by soaking the sample from d in methyl alcohol for 60 minutes, drying in air, and then subjecting it to a heating schedule similar to that depicted by curve t. The effect of liquid nitrogen alone was tested by soaking the sample from run e in liquid nitrogen, letting it warm to room temperature in air, and making run f.

D. Discussion of Non-Steady State Behavior

The atomically plane cleaved surface appears to be unique in that it is a tremendous hinderance to the motion of evaporation ledges. It could not be determined with any certainty whether this was due to a contaminated surface, a natural consequence of the interaction between the steady state sublimation kinetics and the nature of the cleaved surface, or a combination of the two.

The most likely sources for surface contamination are impurity adsorption incurred during the handling at atmospheric conditions, the cleavage in liquid nitrogen, the transfer from the nitrogen to the alcohol, and the soak in the alcohol bath. The experiments summarized in Fig. 21 show that contamination of the surfaces reduced the rate of approach to steady state sublimation. But contamination of a surface which had reached its steady structure in no case produced as long a

delay in reaching steady state as the 245 minute period observed with the original cleaved surface. An induction period of 50 to 80 minutes can be associated with contamination of a steady state surface, and the long induction period is in some way associated with the nature of the cleaved surface.

It seems probable that the difference arises because the surface energy of a cleaved surface is higher than that for the equilibrium or near equilibrium surface developed during steady state sublimation. The experiments of Fig. 21 show clearly that contamination by air and by the reagents used in sample preparation reduce the rate at which a previously heated sample approaches its steady state upon reheating. The non-equilibrium surface of a newly cleaved sample should adsorb the same impurities much more strongly than does a sample whose surface is at or near equilibrium with the bulk, and these were more strongly adsorbed impurities which could provide efficient impedence to zinc sublimation.

The different types of pits illustrated on Figs. 23-a and 25 might have formed at dislocations of different character. Ellis[67] has shown that chemical etch pits in germanium could be classified into distinct types by appearance, and he concluded that the different types probably reflected a difference in the screw and edge components of the dislocation.

The difference between the long straight ledges formed during the initial pitting of the high purity zinc and the irregular ledges formed on the grown zinc may be due to the different impurity concentrations.

VI. SUMMARY OF OBSERVATIONS AND CONCLUSIONS

It seems appropriate in summary to review briefly the observations which have been made on zinc sublimation and to suggest possible mechanistic interpretations. An effort will be made to indicate the strength or weakness of evidence in support of each interpretation.

The (0001) zinc surfaces when freshly cleaved, sublime at initial rates about two orders of magnitude lower than their steady state rates. The rate of sublimation varies in the initial non-steady state region in a manner that is clearly correlated with the increase in dimensions of pits that form in the crystal surfaces and if the edges are not masked, at crystal edges as well. The initial thermal pits are probably formed at places where dislocations intersect the surface, although it is not proven conclusively. An undetermined set of variables determine whether a thermal pit forms at a dislocation or not, and on the average only one out of every 10 - 20 dislocations seems to produce a thermal pit.

Exposure of crystal surfaces that have the structure characteristic of steady state sublimation to air, methyl alcohol, and liquid nitrogen all cause non-steady state sublimation behavior of freshly cleaved samples. But the time to reach steady state a second time is less, regardless of which reagent the surface is exposed to.

Observation of the steepness of pit walls near the (0001) surface indicates that surface ledges can progress only at much slower rates than ledges within the pits. These observations are consistent with the interpretation that steady state sublimation is obtained only when an adsorbed layer of various impurities has been broken and stripped away by advancing crystal ledges. Adsorption of any given impurity such as

oxygen or water should be stronger on the non-equilibrium cleaved surfaces than on the near equilibrium surfaces developed during steady state sublimation. As a consequence the rate of approach to the steady state is hindered by both the absence of ledge sites from which zinc atoms can move to surface adsorption sites and by the impedence provided to ledge advancement by the strongly adsorbed impurities.

The evaporation coefficients for the (0001) and $(10\bar{1}0)$ planes of high purity zinc are unity even when the concentration of actual sources of thermal ledges is less than $10^4/cm^2$. The sublimation flux is surprisingly insensitive to pertubations on the surface such as the formation of oxide particles and gaseous contamination. On the other hand, bulk impurities apparently play a very influential role in determining the rate of sublimation and the morphological development of the (0001) surface. A total bulk impurity content as low as 0.0013% appears to be responsible for the reduction of α from 1 to 0.7 and to markedly alter the surface morphology. Impurities promote the formation of pits and ledges upon evaporation, features which are not seen on the surface of high purity zinc.

The edges of the crystal are established as being very ready sources of evaporation steps and ledges. When the edges of the grown crystal are masked, evaporation ledges readily form at pit sources, which are presumably related to dislocations. However, the flux of sublimation is not directly dependent upon the number of active pits on the surface. The pits from which ledges emanate on the (0001) surface of the grown zinc and are rendered unimportant once the edges of the crystal are exposed.

The importance of dislocations in the evaporation mechanism of simple metals is not established with any certainty. A variation of the dislocation density over an order of magnitude has no noticeable effect on the experimental evaporation coefficient. The results of this investigation are in apparent disagreement with the Hirth and Pound prediction that α equals 1/3 for low index surfaces with less than 10^6 dislocations/cm^2. A coefficient of unity was observed for dislocation densitites ranging from 3×10^4 to 2×10^5 lines/cm^2.

ACKNOWLEDGEMENTS

The author wishes to express his sincere thanks to Prof. Alan W. Searcy for his guidance and counsel throughout the course of this investigation. Thanks are also extended to Dr. David J. Meschi and my fellow graduate students for their numerous suggestions and comments. The author also acknowledges the fine support given by various members of the Lawrence Radiation Laboratory staff. Gratitudes are extended to George Georgakopoulos for his help with the electron microprobe, Prof. Thomas E. Everhart for the use of his scanning electron microscope, Mide Nemienac for his assistance in using the electron microscope, and Lexie Anderson for typing the manuscript. Finally, the author is deeply appreciative of the understanding and encouragement given by his wife, Joanne.

This work was performed under the auspices of the United States Atomic Energy Commission.

REFERENCES

1. H. Hertz, Ann. Phys. 17, 177 (1882).
2. M. Knudsen, Ann. Phys. 47, 697 (1915).
3. Z. A. Munir and A. W. Searcy, J. Chem. Phys. 42, 4223 (1965).
4. R. D. Schultz and A. V. Dekker, J. Phys. Chem. 66, 1095 (1950).
5. G. A. Somorjai and J. E. Lester, in Progress in Solid State Chemistry (Pergamon Press, Oxford, England, 1967), H. H. Reiss, ed.
6. M. Volmer, Kinetic der Phasenbildung, Dresden and Leipzig, 1939.
7. W. Kossel, Nachr. Ges. Wiss, Gottingen, 135, (1927).
8. I. N. Stranski, Z. Phys. Chem. 136, 259 (1928); B4, 121 (1931).
9. O. Knacke and I. N. Stranski, Ergebn. exakt. Naturwiss. 26, 414 (1952).
10. O. Knacke and I. N. Stranski, Prog. Met. Phys. 6, 181 (1956).
11. J. P. Hirth and G. M. Pound, J. Chem. Phys. 26, 1216 (1957).
12. J. P. Hirth and G. M. Pound, J. Phys. Chem. 64, 619 (1960).
13. J. P. Hirth and G. M. Pound, Acta Met. 5, 649 (1957).
14. F. C. Frank, Disc. Faraday Soc. 5, 48, 67 (1949).
15. N. Cabrera and W. K. Burton, Disc. Faraday Soc. 5, 33, 40 (1949).
16. A. R. Verma, Crystal Growth and Dislocations (Academic Press Inc., New York, 1953).
17. N. Cabrera and M. M. Levine, Phil. Mag. 1, 450 (1956).
18. B. Paul, ARS Journal, 32, 1321 (1962).
19. J. P. Hirth and G. M. Pound, Prog. in Mat'ls. Sci. 11, (1963).
20. J. P. Hirth and G. M. Pound, Trans. A.I.M.E. 215, 932 (1959).
21. A. A. Jones, Il Langmuir, and G. M. J. Mackay, Phys. Rev. 30, 201 (1927).
22. E. A. Gulbransen and K. E. Andrews, J. Electrochem. Soc. 66, 442 (1942).

23. R. Schuman and R. B. Garrett, J. Am. Chem. Soc. 66, 442 (1942).

24. L. G. Carpenter and W. N. Mair, Trans. Faraday Soc. 55, 1924 (1959).

25. F. Metzger, Helv. Phys. Acta. 16, 323 (1943).

26. L. G. Carpenter and W. N. Mair, Proc. Phys. Soc. 614, 57 (1951).

27. G. Wessel, Z. Physik, 130, 539 (1951).

28. W. L. Winterbottom, and J. P. Hirth in Condensation and Evaporation of Solids (Gordon and Breach, New York, 1962) p. 347.

29. R. B. Holden, R. Speiser, and H. L. Johnston, J. Am. Chem. Soc. 70, 3897 (1948).

30. J. W. Edwards, H. L. Johnston and W. E. Ditmars, J. Am. Chem. Soc. 75, 2467 (1953).

31. O. M. Poltarkak and G. P. Panasyuk, Zhur. Fiz. Khim. 31, 2644 (1957).

32. F. E. Dart, Phys. Rev. 78, 761 (1950).

33. H. S.Rosenbaum and M. M. Saffen, J. Appl. Phys. 32, 1866 (1961).

34. J. V. Sharp. Phys. Stat. Solidi, 8, K1 (1965).

35. A. W. Ruff, J. Chem. Phys. 41, 1204 (1964).

36. R. W. Mar and A. W. Searcy, J. Phys. Chem. 71, 888 (1967).

37. H. Skinner and A. W. Searcy, J. Phys. Chem. in press.

38. H. Mayer, Z. Physik, 67, 240 (1931).

39. M. Vollmer, Z. Physik Chem., Bodenstein Festband, 803 (1931).

40. R. D. Freeman and A. W. Searcy, J. Chem. Phys. 22, 762 (1954).

41. R. D. Freeman, ASD-TDR-63-734, 1960.

42. C. L. McCabe, and C. E. Birchenall, A.I.M.E. Trans. 197, 707 (1953).

43. J. Fischer, Z. Anorg. Allgem. Chem. 119, 1 (1934).

44. P. Grieveson, C. W. Hopper, and C. B. Alcock, Physical Chemistry of

Process Metallurgy (Interscience Publishers, New York, 1961).

45. D. R. Stull and G. C. Sinke, Thermodynamic Properties of the Elements (American Chemical Society, Washington D. C., 1956).

46. R. Hultgren, R. L. Orr, P. D. Anderson, and K. K. Kelly, Selected Values of Thermodynamic Properties of Metals and Alloys (John Wiley and Sons, Inc., New York, 1963).

47. O. Kubaschewski, E. Evans, and C. B. Alcock, Metallurgical Thermochemistry (Pergamon Press, New York, 1967).

48. W. J.Moore and J. K. Lee, Trans. Faraday Soc. 47, 501 (1951).

49. N. Pilling and R. Bedworth, J. Inst. Metals, 29, 534 (1923).

50. C. Gemsch and K. Hauff, Z. Phys. Chem. 196, 427 (1950).

51. W. Vernon, E. Aberoyd, and E. Stroud, J. Inst. Metals, 65, 301 (1937).

52. V. O. Nwoko, and H. H. Uhlig, J. Electrochem. Soc. 112, 1181 (1965).

53. F. C. Frank, in Growth and Perfection of Crystals (John Wiley and Sons, Inc., New York, 1958) R. H.Doremus, B. W. Roberts and D. Turnbull, eds., p. 411.

54. C. Herring, Metal Interfaces (A.S.M. Cleveland, 1952).

55. H. Suzuki, J. Phys. Chem. (Japan), 10, 881 (1955).

56. E. Votava and S. Amelinckx, Naturwissen. 41, 422 (1950).

57. E. Votava, Z. Met. 47, 309 (1950).

58. J. C. Danko and A. J. Griest, J. of Metals, 8, 515 (1956).

59. F. W. Young and A. T. Gwathney, J. Appl. Phys. 31, 225 (1960).

60. G. Wyon and P. Lacombe, Rept. Conf. Defects in Crystalline Solids, London, 1954, p. 187 (1955).

61. F. C. Frank, in Growth and Perfection of Crystals (John Wiley and

Sons, Inc., New York, 1958) R. H. Doremus, B. W. Roberts and D. Turnbull, eds., p. 3.

62. G. M. Rosenblatt, P. K. Lee, and M. B. Dowell, J. Chem. Phys. 45, 3454 (1966).

63. J. P. Hirth and L. Vassamillet, J. Appl. Phys. 29, 595 (1958).

64. A. A. Hendrickson and E. S. Machlin, Acta Met. 3, 64 (1955).

65. M. J. Fraser, D. Caplan and A. A. Burr, Acta Met. 4, 186 (1956).

66. E. Votāva and A. Berghezan, Acta Met. 7, 6 (1959).

67. G. Ellis, J. Appl. Phys. 26, 1140 (1955).

This report was prepared as an account of Government sponsored work. Neither the United States, nor the Commission, nor any person acting on behalf of the Commission:

A. Makes any warranty or representation, expressed or implied, with respect to the accuracy, completeness, or usefulness of the information contained in this report, or that the use of any information, apparatus, method, or process disclosed in this report may not infringe privately owned rights; or

B. Assumes any liabilities with respect to the use of, or for damages resulting from the use of any information, apparatus, method, or process disclosed in this report.

As used in the above, "person acting on behalf of the Commission" includes any employee or contractor of the Commission, or employee of such contractor, to the extent that such employee or contractor of the Commission, or employee of such contractor prepares, disseminates, or provides access to, any information pursuant to his employment or contract with the Commission, or his employment with such contractor.